Increased North African Dust Fluxes and Higher Productivity in the Eastern Equatorial Atlantic Ocean linked to stronger trade winds from about 2.7 Million Years Ago

Anya J. Crocker[1], Amy M. Jewell[1], Bryce A. Mitsunaga[2], Solana Buchanan[2,3], Anieke Brombacher[1,4], Bastian Hambach[1], Megan R. Wilding[1], Thomas Westerhold[5], Ursula Röhl[5], James M. Russell[2], Timothy D. Herbert[2], Chuang Xuan[1], Paul A. Wilson[1]

[1]University of Southampton, Waterfront Campus, National Oceanography Centre, Southampton, United Kingdom

[2]Department of Earth, Environmental, and Planetary Sciences, Brown University, Providence, U.S.A.

[3]Earth, Environmental, and Planetary Sciences, Rice University, Houston, U.S.A.

[4]Department of Earth and Planetary Science, Yale University, New Haven, U.S.A.

[5]MARUM—Center for Marine Environmental Sciences, University of Bremen, Bremen, Germany

Corresponding author: Anya Crocker (ajc1g08@soton.ac.uk)

Key Points:

- We present new records of sea surface temperatures, foraminiferal stable isotopes and export production from the Tropical Atlantic.
- High latitude cooling and steepening meridional temperature gradients drove two phases of aridification/increased African dust export.
- Strengthening trade winds linked to latitudinally variable export productivity responses across the Plio-Pleistocene transition.

Abstract

For at least the last 11 million years, the North African landscape has repeatedly oscillated on astronomical timescales between the dry dusty conditions of today and more humid, vegetated conditions such as those documented for the mid-Holocene. These changes were primarily driven by expansion and contraction of the tropical rainbelt in response to changes in summer insolation. However, other mechanisms are needed to explain temporal variability in the sensitivity of African humidity to this rhythmic forcing. A main interval of observed change is the Pliocene-Pleistocene transition (~3.5 to 2.4 Ma) when Africa is widely (but not universally) suggested to have become drier and dustier. Here we present new suborbitally resolved records of surface ocean temperature, foraminiferal stable isotopes and export productivity from the Northwest African margin and the eastern equatorial Atlantic Ocean and compare them to published records. We find strong coupling at astronomical timescales between productivity and dust fluxes throughout our study interval, indicating the sustained influence of the northeast trade winds on dust transport, upwelling strength and perhaps dust-driven ocean fertilization. We attribute observed increases in dust fluxes delivered to the NW African margin and eastern equatorial Atlantic to strengthening of the trade winds driven by the steepening latitudinal temperature gradients associated with the intensification of Northern Hemisphere glaciation. Taken together with published evidence of increased strength in the mid-latitude westerlies at this time, our results point to invigoration of large-scale atmospheric circulation globally during intensified glacial periods of the Pliocene-Pleistocene transition.

Plain Language Summary

The Sahara has repeatedly grown and shrunk for at least 11 million years, switching between an intensely dusty expanse and a much greener environment with abundant vegetation and extensive networks of rivers and lakes. These changes are paced by subtle variability in the Earth's orbit around the sun, however, the intensity of the resulting arid and humid periods is strongly influenced by global climate. One key example of this occurred approximately three million years ago, when dusty intervals on North Africa became much more intense, approximately coincident with a large increase in ice volume in the northern hemisphere. Here, we present new records of surface ocean temperature and marine productivity from two sites in the tropical Atlantic Ocean to explore the influence that ocean temperatures had in driving these increased dust fluxes. We find that high latitude cooling drove a strengthening of the trade winds, likely as part of a larger-scale global invigoration of atmospheric circulation. These strengthened winds drove differing responses in the productivity of our two study sites. Our results highlight the importance of high latitude influences on both North African rainfall patterns and the highly productive marine ecosystems that sustain local fishing communities.

1 Introduction

Anthropogenic warming is projected to cause large-scale shifts in precipitation patterns. At the global scale, wet regions and seasons are predicted to become wetter and dry ones drier in response to a combination of increased moisture-holding capacity of warmer air, increased rainout efficiency at low latitudes and a poleward expansion of the Hadley cell (Held and Soden,

2006; Scheff and Frierson, 2012; Trenberth, 1998). However, it is increasingly apparent that a universal subtropical precipitation decline is an overly simplistic projection, especially over the continents (Byrne and O'Gorman, 2015; Greve et al., 2014; He and Soden, 2017). In fact, even the sign of predicted rainfall change over land is uncertain in some regions (Monerie et al., 2017; Zhang and Li, 2022).

One region which is particularly sensitive to any rainfall variability is the North African Sahel, which suffered devastating droughts during the 1970s and 1980s (e.g. Ali and Lebel, 2009), and some evidence suggests that a longer-term drying of North Africa is already underway (Thomas and Nigam, 2018; Zhang et al., 2007). However, Sahelian precipitation has increased since the 1980s (Ali and Lebel, 2009; Berntell et al., 2018) and many climate models predict significant regional heterogeneity, with a wetter central Sahel and drier west (Akinsanola and Zhou, 2019; Han et al., 2023; Monerie et al., 2017; Zhang and Li, 2022). Recovery of annual rainfall amounts in the Sahel from drought conditions (although not yet to pre-1970s levels) is attributed to (i) increased greenhouse gas emissions, (ii) decreased anthropogenic aerosol emissions from North America and Western Europe and (iii) surface warming of the North Atlantic Ocean and Mediterranean Sea (Giannini and Kaplan, 2019; Hagos and Cook, 2008; Park et al., 2016). Of these three factors, we can be confident that the impacts of (i) will likely dominate anthropogenic aerosol forcing in the coming decades, but predicting the way in which sea surface temperature (SST) fields will change and the resulting influence on precipitation patterns is far from straightforward. These observations therefore provide a powerful incentive to improve our understanding of records of past change.

Records of palaeoclimate variability from the recent geological past show that, between about 60 and 15 thousand years ago (ka), North Africa was even drier and dustier than today, especially during short intervals when millennially paced disruptions to Atlantic Meridional Overturning Circulation (AMOC) instigated intense cooling of the surface North Atlantic Ocean (e.g. Collins et al., 2013; Kinsley et al., 2022; Mulitza et al., 2008). Records of the recent past also show that precession-paced peaks in summer insolation during interglacial conditions triggered distinctly humid intervals in North Africa, resulting in a vegetated North African landscape with extensive lakes and northward-draining river systems (e.g. Drake et al., 2011; Hély and Lézine, 2014; Larrasoaña et al., 2013), which triggered rapid increases in dust emissions when these systems later dried out (Ehrmann and Schmiedl, 2021). However, IPCC-class climate models consistently fail to reproduce early Holocene greening of the Sahara (Brierley et al., 2020), posing serious questions about the reliability of future forecasts and raising the alarming possibility that these models are artificially stable because of the way in which their uncertain parameterizations are tuned (Hopcroft and Valdes, 2021).

Intervals of low northern hemisphere summer insolation and the millennially paced cold North Atlantic intervals were also typically associated with a strengthening of trade winds, driving increased dust export from North Africa (e.g. Kinsley et al., 2022; McGee et al., 2013; O'Mara et al., 2022; Skonieczny et al., 2019) and increased upwelling along the Northwest African margin, bringing cooler, nutrient-rich waters to the surface and increasing biological productivity (Adkins et al., 2006; Bradtmiller et al., 2016; Romero et al., 2008). Thus, the late Quaternary geological record indicates strongly coupled behaviour between ocean and atmospheric dynamics in North Africa. Yet, while these observations provide valuable context, they only offer indirect insight into the African climate response to the levels of greenhouse gas

forcing that Earth will experience in the coming decades. Longer palaeoclimate records are needed, reaching back into the pre-Pleistocene to intervals when greenhouse gas concentrations last reached the anthropogenically perturbed levels observed today and for which, unlike today, the atmosphere was equilibrated, resulting in global temperatures ~2–3°C warmer than present (de la Vega et al., 2020; McClymont et al., 2020). The transition from the warm Pliocene to the cooler Pleistocene (3.3–2.4 Ma) was marked by an expansion of ice volume, particularly in the northern hemisphere, decreasing atmospheric pCO_2 concentrations and latitudinally-dependent SST cooling across the globe with a strengthening of 41-kyr (obliquity) variability recorded in many climate records associated with an increase in the magnitude of glacial-interglacial cycles (Martinez-Boti et al., 2015; McClymont et al., 2023). This shift in global climate had wide-

ranging impacts both in the ocean and on land, including on rainfall patterns in currently water-stressed regions such as North Africa (e.g. deMenocal, 1995; Feng et al., 2022).

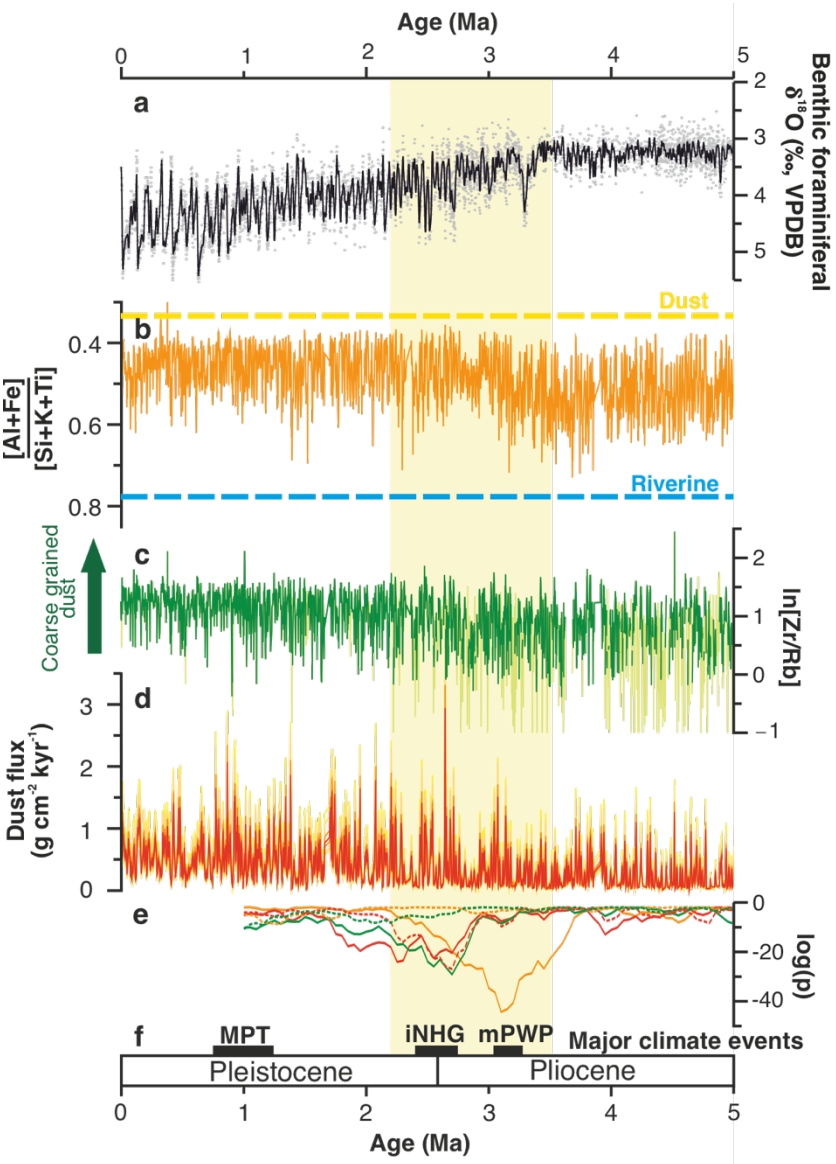

Figure 1. African hydroclimate compared with global change over the past 5 Myr, adapted from Crocker et al. (2022). **a** Cenozoic global reference benthic foraminifera oxygen isotope dataset (CENOGRID, grey points), with 20 kyr smoothing (black line) (Westerhold et al., 2020; Wilkens et al., 2017). **b** [Al+Fe]/[Si+K+Ti] of calibrated elemental abundances from ODP Site 659 (Crocker et al., 2022). Modern endmember values of Saharan dust and Senegal River suspended material updated from Mulitza et al. (2010). **c** ln[Zr/Rb] XRF core scan ratios from ODP Site 659 (Crocker et al., 2022). **d** ODP Site 659 estimated dust flux (3-point smoothed). Median value in red; 1st, 5th, 25th, 75th, 95th and 99th percentiles also shown in shades of orange/yellow (Crocker et al., 2022). **e** log(*p*) values indicating probability of shifts in central tendency (Mann-Whitney-Wilcoxon test , solid lines) and dispersion (Ansari-Bradley test, dashed lines) (Crocker et al., 2022). Low *p*-values indicate extremely low probabilities that the two adjacent 1 Ma data bins

have the same central tendency and/or dispersion, respectively. Colours indicate the analysed proxy data series matching the panels above, with [Al+Fe]/[Si+K+Ti] in orange, ln[Zr/Rb] in green and median dust flux in red. **f** Major climate events: MPT - Mid-Pleistocene Transition, iNHG – intensification of Northern Hemisphere Glaciation, mPWP – mid-Pliocene Warm Period.

North Africa has a long-established history of astronomically paced oscillations between distinctly dry and dusty conditions and more humid ones (e.g. deMenocal, 1995; Grant et al., 2017; Rossignol-Strick, 1985; Sarnthein et al., 1982; Tiedemann et al., 1994). These oscillations were recently shown to i) date from at least 11 million years ago and ii) display amplitude changes, implying changes in the sensitivity of African hydroclimate to insolation associated with changes in global climate state (Crocker et al., 2022, Figure 1). The most recent example of these amplitude changes is shown in Figure 1, where a marked increase in the intensity of both arid phases and dust export is seen across the transition from the warm Pliocene into the cooler Pleistocene, with the increase in aridity predating increasing dust fluxes by ~400 kyr (Crocker et al., 2022; deMenocal, 1995). Here, we explore the cause of this transition, focusing on the role played by coupling between ocean and atmosphere in driving regional hydroclimate, wind strength and the productivity of major upwelling systems. To this aim, we present new records of surface ocean temperature, foraminiferal stable isotope signatures and export productivity from the Northwest African margin and eastern equatorial Atlantic (EEA).

1.1 Site Locations

Our main study location is Ocean Drilling Program (ODP) Site 659, which is situated in the tropical North Atlantic Ocean on the Cape Verde Rise, offshore Mauritania (18.077°N 21.026°W, 3070 m water depth, Figure 2). Here, the Mauritania Current brings warm, oligotrophic surface waters from the south (Lázaro et al., 2005), while to the north of the site, the Canary Current transports relatively cool waters southwards along the African coast before heading southwestwards to join the North Equatorial Current (Mittelstaedt, 1991). We also present new data from ODP Site 662, located in the eastern equatorial Atlantic Ocean, on the upper eastern flank of the Mid-Atlantic Ridge (1.390°S, 11.739°W, 3814m water depth, Figure 2). Here, the surface hydrography is predominately controlled by the westward flowing South Equatorial Current, but the site is also close to the influence of the Atlantic Equatorial

Undercurrent, which transports cool and salty waters westwards at depths of ~50-100m (Johns et al., 2014; Richardson and Walsh, 1986).

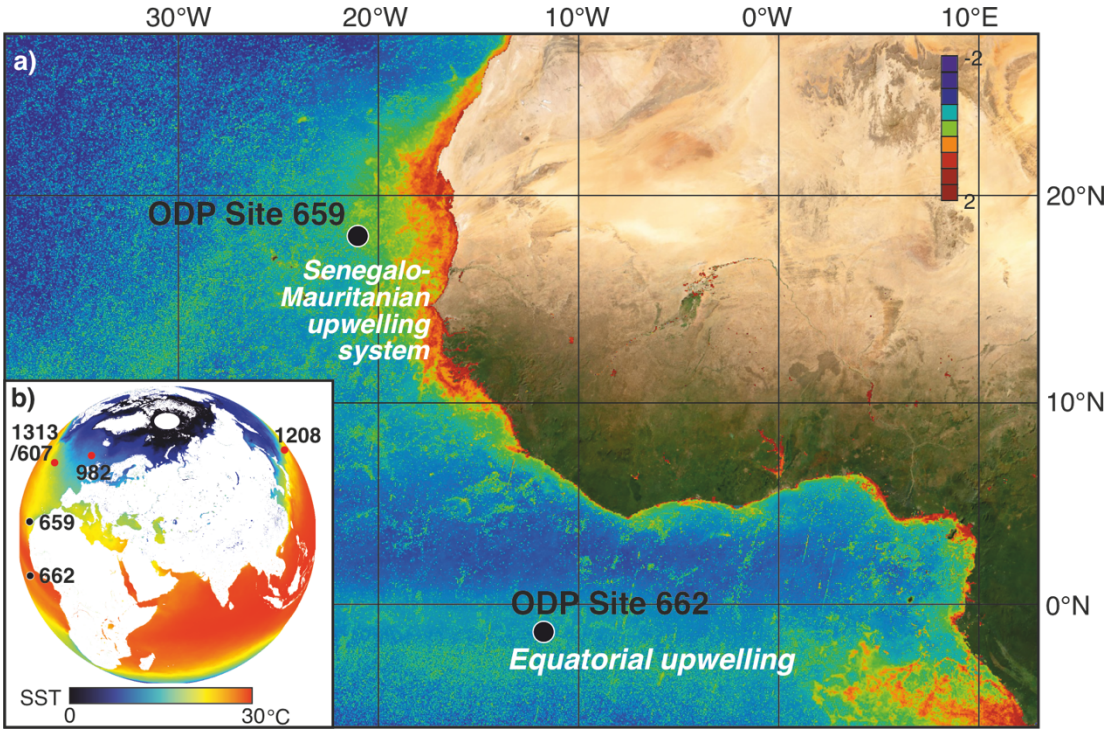

Figure 2. Site locations and surface water mass properties. **a** Locations of studied sites ODP 659 and 662 (black circles). Colour of ocean regions indicates concentrations of green pigment chlorophyll-a in phytoplankton in the sea surface layer, plotted as $\log_{10}[0.016C]$, where C = mean daylight values across 2021 (in mg/m^3), with red shading indicating the most productive regions. Data from Murakami (2020). Satellite images of continents from ESRI world imagery (Esri, 2023). Major upwelling zones labeled in white text. **b** Mean annual sea surface temperatures (°C) in 2021 (Kurihara, 2020), with studied sites shown by black dots and other key sites referred to in the text marked by red dots. Data accessed via Google Earth Engine (Gorelick et al., 2017), and figure created using QGIS (QGIS.org, 2024).

ODP sites 659 and 662 are both influenced by upwelled subsurface waters. ODP Site 659 is located on the fringes of the Senagalo-Mauritanian Upwelling System (Figure 2), in a region that today experiences seasonal upwelling driving high surface water chlorophyll levels from October through May (Lathuilière et al., 2008). This region forms part of the Canary Current Eastern Boundary Upwelling System, which extends along much of the coastline of northwest Africa and is one of the four major Eastern Boundary Upwelling Ecosystems. The ongoing and future response of this upwelling system to increasing global warmth is much debated, with a proposed strengthening of upwelling (Bakun, 1990) receiving mixed support from records showing little or spatially variable change in productivity (Cropper et al., 2014; Fischer et al., 2016), and reconstructions of Late Quaternary climate suggesting that strongest upwelling occurred during glacial periods (e.g. Bradtmiller et al., 2016; Matsuzaki et al., 2011). ODP Site

662 sits within the regional of equatorial upwelling (Figure 2), with a maximum in upwelling strength in June driven by wave upwelling (Wang et al., 2017). Upwelled waters at both sites are largely sourced from South Atlantic Central Water (Hagen and Schemainda, 1987; Mittelstaedt, 1991; Stramma and England, 1999). South Atlantic Central Water forms by subduction in the South Atlantic subtropical gyre (Stramma and England, 1999) and is transported into our study area from the south. It is typically found at depths of ~100–300m and is cooler, fresher and more nutrient-rich than surface waters (Mittelstaedt, 1991; Peña-Izquierdo et al., 2012, Figure 2).

North African climate and continental biomes both show strong latitudinal banding, with ODP Site 659 situated close to the latitude of the present-day Sahara-Sahel boundary. Precipitation over Africa in this region is strongly seasonal. Northward migration of the tropical rainbelt in boreal summer brings rainfall to much of the Sahel through the influence of the West African monsoon and is strongly linked to the seasonal latitudinal transit of the intertropical convergence zone (ITCZ) (Nicholson, 2009). North Africa is also the source of approximately half of the world's atmospheric dust load (Kok et al., 2021), much of which is transported westwards over the Atlantic Ocean. As a result, ODP Site 659 preserves an excellent record of past dust emissions from Africa (Crocker et al., 2022; Tiedemann et al., 1994). Dust deposition occurs year-round, delivered predominantly by the northeast trade winds (NETW) during winter and spring, with additional contributions via the Saharan Air Layer (which transports dust westwards across the Atlantic Ocean) during boreal summer (Skonieczny et al., 2013; Stuut et al., 2005; van der Does et al., 2021). Further south, ODP Site 662 receives dust predominantly during winter and spring, transported by from central North Africa via the NETW when the ITCZ is in a southerly position (Yu et al., 2019)

Both of our study sites are located in elevated positions compared to the surrounding seafloor (ODP Site 659 on the Cape Verde Rise and ODP Site 662 on the flank of the Mid-Atlantic Ridge) and are therefore protected from the influence of major mass transport deposits (Ruddiman et al., 1989). Sediments are dominantly composed of a mixture of nannofossil and foraminiferal oozes (ODP Site 659: 35–90% $CaCO_3$, ODP Site 662: 60–95% $CaCO_3$) and lithogenic material (Ruddiman and Janecek, 1989; Ruddiman et al., 1989; Tiedemann et al., 1994). The lithogenic fraction is interpreted to be dominated by dust at both sites (Ruddiman and Janecek, 1989; Ruddiman et al., 1989; Tiedemann et al., 1994), although grain size data show that ODP Site 659 received a significant fine-grained lithogenic component that is distinct from modern dust inputs, suggesting a distal influence from African (palaeo)rivers during times of past humidity (Crocker et al., 2022).

2 Methods

2.1 Foramiferal calcite stable isotope analysis

Globigerinoides ruber (white) (d'Orbigny, 1839) is a symbiont-bearing, mixed-layer dwelling planktonic foraminiferal species found in tropical and subtropical waters (Ganssen and Kroon, 2000; Tolderlund and Bé, 1971). *G. ruber* (white) occurs throughout the year, but can show a distinct seasonality in abundance and/or depth habitat depending upon local hydrography

(Peeters et al., 2002; Tolderlund and Bé, 1971). *G. ruber* (white) is also able to tolerate low salinities associated with large freshwater inputs (e.g. Curry et al., 1983).

Foraminiferal preservation at ODP Site 659 is generally good, with very limited recrystalisation and little infilling of pores. For each foraminiferal carbonate stable isotope analysis, 50 specimens of *G. ruber* (white) were picked from the 212–250 μm size fraction. Foraminiferal tests were gently broken open and cleaned by ultrasonification in methanol. Aliquots of ~25–45 μg of calcite for each sample were analysed at the University of Southampton's Waterfront Campus using the Thermo Scientific Kiel IV Carbonate Device coupled with a MAT253 isotope ratio mass spectrometer. All values of oxygen and carbon isotope composition are expressed in delta notation, relative to Vienna Peedee Belemnite standard, with an external precision of 0.04 ‰ for $\delta^{13}C$ and 0.08 ‰ for $\delta^{18}O$. We also picked and analysed epifaunal benthic foraminiferal species *Cibicides wuellerstofi* from the 250–300 μm size fraction in a subset of samples in a gap in the existing oxygen isotope stratigraphy (Tiedemann et al., 1994), allowing us to identify Marine Isotope Stage M2 (at ~3.3 Ma), the largest late Pliocene glacial prior to the intensification of Northern Hemisphere glaciation (iNHG).

2.2 Alkenone fluxes and estimation of SST

Biomarkers were extracted from freeze dried, homogenized sediment via a Thermo Scientific (Dionex) Accelerated Solvent Extractor (models 200 and 350) in 9:1 methylene chloride (DCM): methanol and purified via flash silica gel column chromatography involving sequential hexane, DCM, and methanol rinses. Peak areas of compounds in the ketone-containing DCM fraction were quantified by an Agilent 6890 gas chromatography flame ionization detector outfitted with an Agilent VF-200 column using the TEXPRESS software (Dillon and Huang, 2015) and converted to concentrations via an internal 36- and 37-carbon *n*-alkane spike.

The ratio of $C_{37:3}$ and $C_{37:2}$ methyl alkenones ($U^{k'}_{37}$) was used to calculate SST based on the calibration of Müller et al. (1998). 10 samples were duplicated and differences between replicates were generally within 0.2°C. We also report fluxes of the C_{37} alkenone (C_{37} flux) which are representative of surface ocean productivity in upwelling-influenced areas (Bolton et al., 2010).

2.3 Local seawater $\delta^{18}O$ estimation

We applied the species-specific equation of Mulitza et al. (2003) to estimate seawater $\delta^{18}O$ values ($\delta^{18}O_{sw}$) from *G. ruber* (white) $\delta^{18}O$ and alkenone-derived SST values. An offset adjustment of 0.27‰ was applied to convert values to the vSMOW scale (Coplen, 1988; Hut, 1987). To better reconstruct local changes in the precipitation-evaporation balance, we also adjust for global changes in $\delta^{18}O_{sw}$ related to changes in the volume and isotopic composition of major ice sheets. We use three different approaches to adjust for past change in global $\delta^{18}O_{sw}$ compositions (to assess the impact of some of the uncertainties involved, such as the potential influence of deep water temperature change on benthic foraminiferal $\delta^{18}O$), as follows: 1)

reconstructing global $\delta^{18}O_{sw}$ from the benthic foraminiferal oxygen isotope stack LR04 (Lisiecki and Raymo, 2005), following the method of Karas et al. (2009). 2) Reconstructing global $\delta^{18}O_{sw}$ from estimates of past sea level calculated using an inverse modelling approach including 3D ice-sheet modelling with climate forcing from general circulation models (Berends et al., 2021) and converting these values to seawater oxygen isotope values assuming a linear relationship between sea level and global average $\delta^{18}O_{sw}$ of 0.011‰ m^{-1} (Fairbanks, 1989; Raymo et al., 2018). 3) Using the process-model based Plio-Pleistocene synthesis median global $\delta^{18}O_{sw}$ values of Rohling et al. (2022), which incorporate a non-linear relationship between sea level and $\delta^{18}O_{sw}$.

There are multiple sources of uncertainty incorporated within the $\delta^{18}O_{sw}$ estimates in addition to the uncertainty in estimates of global seawater $\delta^{18}O_{sw}$ driven by changes in ice volume discussed above. Both the $\delta^{18}O_{calcite}$ and SST values used to calculate $\delta^{18}O_{sw}$ have their own analytical uncertainties (0.08 ‰ and 0.2°C respectively). There is also uncertainty in the conversion of $U^{k'}_{37}$ values into absolute temperatures, estimated as ~1.5°C in the calibration of Müller et al. (1998) used here, although other studies have suggested that uncertainty could be as large as 4.4°C at high temperatures (Tierney and Tingley, 2018). $\delta^{18}O_{sw}$ estimates may also be impacted by seasonality and/or differences in water depth in one or both of the proxy carriers. Alkenone-derived SST estimates have shown to be representative of surface (or very near surface) temperatures (e.g. Herbert, 2001; Sikes et al., 1991), while *G. ruber* are known to be mixed-layer dwellers typically found within the uppermost ~60 m of the water column (e.g.Jentzen et al., 2018; Peeters et al., 2002). Production (and depth habitiat) of both alkenones and *G. ruber* can show strong seasonality (e.g. Rosell-Melé and Prahl, 2013; Tolderlund and Bé, 1971; Volkman, 2000), however, offshore northwest Africa, there appears to be little seasonality in modern alkenone production (Müller and Fischer, 2001) and any seasonal effects on *G. ruber* $\delta^{18}O$ appear to be small (Jonkers and Kučera, 2015; Steph et al., 2009; Wang et al., 1995; Wit et al., 2010).

2.4 Total Organic Carbon (TOC%)

Total organic carbon contents were calculated for a subset of samples to compare to XRF-based proxies for organic carbon content. Bulk sediment samples were crushed and then decarbonated. Organic carbon concentrations of the decarbonated samples were analysed using an Elementar vario Isotope Select Elemental Analyzer equipped with a thermal conductivity detector (standard deviation = 0.06%). $\%CaCO_3$ contents were measured using a UIC CM5015 CO_2 Coulometer with AutoMate Prep Device (long-term precision = 0.97%), and these values were then used to calculate TOC% of the raw bulk sediment (i.e. prior to decarbonation). All analyses were carried out at the University of Southampton's Waterfront Campus.

2.5 X-ray fluorescence (XRF) core scanning

Most of the XRF core scan data from ODP Site 659 shown here were originally presented in Crocker et al. (2022) where a full methodology can be found. Here we present a record of

bromine (Br) counts from ODP Site 659 for the first time alongside both Br and barium (Ba) counts from ODP Site 662. All sections were analysed using the XRF Core Scanner II (AVAATECH Serial No. 2) at MARUM - University of Bremen with measurements taken every 5 cm down core and count times of 20 seconds. Br was measured using generator settings of 30 kV and 0.75 mA current, while 50 kV and 1 mA were used for Ba counts. The split core surface was covered with a 4 micron thin SPEXCerti Prep Ultralene foil to avoid contamination of the XRF measurement unit and desiccation of the sediment. The data were acquired using a Canberra X-PIPS Silicon Drift Detector (Model SXD 15C-150-500) with 150eV X-ray resolution, the Canberra Digital Spectrum Analyzer DAS 1000, and an Oxford Instruments 50W XTF5011 X-Ray tube with rhodium target material. Raw X-ray spectra were processed using an iterative least square software (WIN AXIL) package from Canberra Eurisys. Repeat runs of several core sections were used to correct for any drift in counts over time.

Br counts obtained by XRF core scanning provide a proxy for total organic carbon content of marine sediments in regions with low terrestrial carbon inputs because of the association of Br with marine organic matter (Ziegler et al., 2008), although Br can also be removed by post-depositional oxidation in some settings (Price and Calvert, 1977). Ba counts are also a powerful proxy for oceanic productivity in many settings, although can be susceptible to remobilization during diagenesis (and secondary contributions from the lithogenic fraction) (e.g. Dymond et al., 1992; Martinez-Ruiz et al., 2000). Both Ba and Br counts are expressed as ratios over total XRF counts (tot) to minimize the impact of variable fluxes of lithogenic material or calcium carbonate. These ratios show very strong agreement with total organic carbon concentrations (TOC%) (supplementary figure 1). Both sedimentary organic matter and Br can be removed by post-depositional oxidation in some settings (e.g. Arndt et al., 2013; Canfield, 1993; Price and Calvert, 1977), while C_{37} alkenones are comparatively (although not completely) resistant to degradation (Grimalt et al., 2000). Very strong agreement between the upwelling/export productivity proxies (XRF-based ln[Br/tot] and ln[Ba/tot], C_{37} flux) at ODP sites 659 and 662 (Figures 3 & 4) therefore supports the use of Ba and Br as palaeoproductivity indicators, and suggests that diagenesis is not a major influence on the down core variability in these elements at our study sites, although variability in C_{37} flux is generally of much lower amplitude than Ba and Br prior to ~2.7 Ma.

To estimate dust fluxes to ODP Site 659, the XRF core scan data were calibrated using discrete samples using a multivariate log calibration approach (Weltje et al., 2015) to obtain major element concentrations. Dust proportions were then estimated using an endmember unmixing approach largely following the method of Mulitza et al. (2010) (see Crocker et al. (2022) for full method details). Estimated dust fluxes show very good agreement with Th-normalised dust fluxes from a nearby site (supplementary figure 2), suggesting that the dust flux reconstructions are representative of aeolian transport from the continent and not major sediment redistribution in the ocean or rapid pulses of dissolution, at least over the last 250 kyr (see Crocker et al., 2022 for full details). The ratio [Al+Fe]/[Si+K+Ti] (with calibrated elemental abundances) is also used as a proxy for continental hydroclimate, with lower values indicating a dominance of aeolian inputs over riverine material (Crocker et al., 2022; Mulitza et al., 2010).

This ratio agrees well with plant wax deuterium isotope signatures from the same site (Kuechler et al., 2018; Kuechler et al., 2013), supporting its use as a hydroclimate proxy.

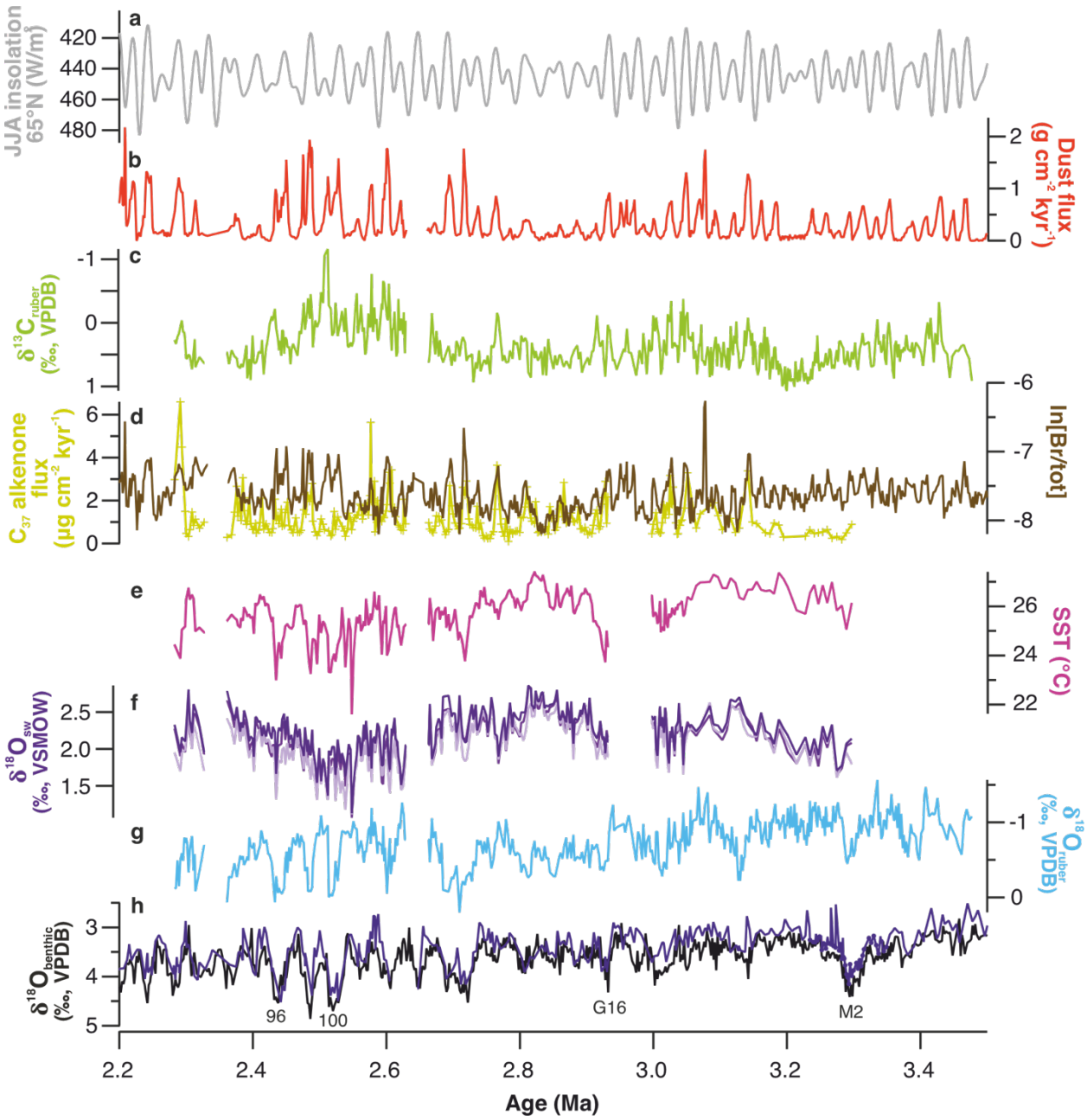

Figure 3. Productivity and organic matter proxies compared to dust fluxes at ODP Site 659. **a** Summer (June, July & August) insolation at 65°N (La2004 solution, in grey) (Laskar et al., 2004). **b** Median dust flux at ODP Site 659 (Crocker et al., 2022). **c** Carbon isotopic signatures ($\delta^{13}C$) of mixed layer species *G. ruber* (white) at ODP Site 659. **d** Flux of C_{37} alkenones (mustard yellow) and ln[Br/tot] counts measured by XRF core scanning (brown), both at ODP Site 659. e Alkenone-derived SST estimates at ODP Site 659 (dark blue). **f** Estimated $\delta^{18}O_{sw}$ at ODP Site 659 calculated using three different approaches to correct for global ice volume change on ocean $\delta^{18}O$, with method (1) in palest purple, method (2) in intermediate shade and method

(3) in darkest purple (see section 2.3). **g** $\delta^{18}O$ of *G. ruber* (white) from ODP Site 659 (sky blue). ODP Site 659 benthic foraminiferal (*C. wuellerstorfi*) oxygen isotope record (dark blue line), with published data from Tiedemann et al. (1994) placed onto our updated stratigraphy and combined with new analyses (blue dots) into a single record. Also shown is CENOGRID benthic foraminfera oxygen isotope dataset (black), with key marine isotope stages (MIS) labelled (Westerhold et al., 2020; Wilkens et al., 2017).

2.6 Stratigraphy

The stratigraphy used in this study largely follows that published by Crocker et al. (2022). A spliced composite section was generated by correlating core images and XRF core scan data between holes A–C drilled at Site 659 using the Code for Ocean Drilling Data macros (Wilkens et al., 2017). The age model was developed by tuning ln[Ca/Fe] ratios to summer insolation (June-July-August) at 65°N in the La2004 astronomical solution (Laskar et al., 2004), also guided by correlation between *C. wuellerstorfi* oxygen isotope values (Tiedemann et al., 1994 and this study) and the LR04 benthic oxygen isotope stack (Lisiecki and Raymo, 2005) and updated paleomagnetic, nannofossil and planktonic foraminiferal datums (Ogg, 2012; Raffi et al., 2006; Ruddiman et al., 1989; Wade et al., 2011). Summer insolation at 65°N was chosen as a tuning target due to its strong obliquity component which makes it excellent match to records of North African monsoon variability preserved by Mediterranean sapropels (Bosmans et al., 2015; Hilgen et al., 1995; Lourens et al., 1996; Tuenter et al., 2003). The use of an astronomically-tuned age model does not have a major impact on the periodicities of variability recorded at this site (see Crocker et al., 2022).

The stratigraphy presented here contains one adjustment to the splice and several minor adjustments to the age model between 2.406 and 2.716 Ma (68.95–79.14 m CCSF) to that originally presented in Crocker et al. (2022). Our new benthic oxygen isotope data indicated that no further refinements to the age model were required around MIS M2 (~3.3 Ma). There is some coring disturbance in a thin interval within 659B 10H spanning from section 2 61cm to section 3 143cm (85.27–87.59 CCSF) which degrades the orbital signal preserved in that interval, but we

include data from the impacted interval because no stratigraphically equivalent sediments were recovered at the site.

All data from ODP Site 662 are plotted on the age model of Herbert et al. (2010), which is based on correlation of benthic foraminiferal oxygen isotope to the LR04 global stack (Lisiecki and Raymo, 2005).

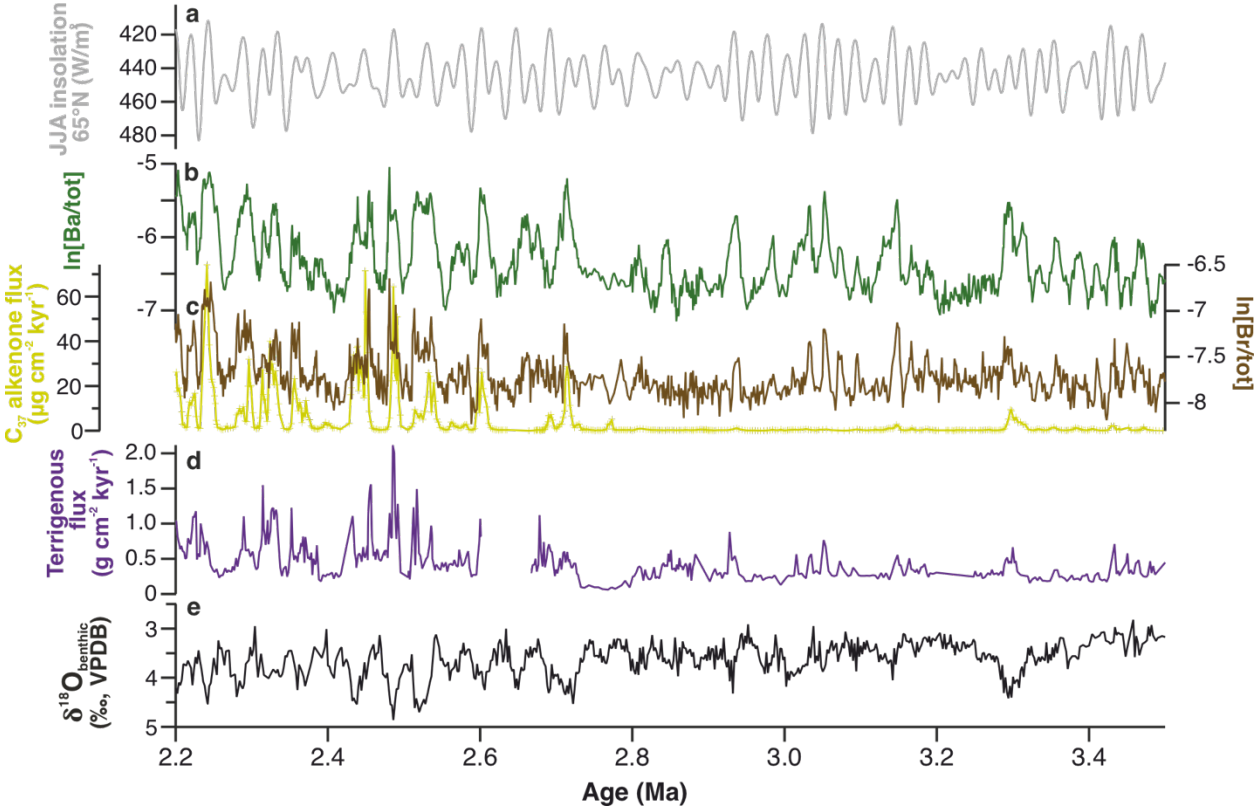

Figure 4. Productivity and organic matter proxies compared to terrigenous fluxes at ODP Site 662. **a** Summer (June, July & August) insolation at 65°N (La2004 solution, in grey) (Laskar et al., 2004). **b** ln[Ba/tot] counts measured by XRF core scanning (dark green). **c** Flux of C_{37} alkenones (mustard yellow, Lawrence et al. (2013)) and ln[Br/tot] counts measured by XRF core scanning (brown, this study), both at ODP Site 662. **d** Terrigenous flux at ODP Site 662 (dark blue), with data from Ruddiman and Janecek (1989) updated to the stratigraphy of Herbert et al. (2010). **e** CENOGRID benthic foraminfera oxygen isotope dataset (black) (Westerhold et al., 2020; Wilkens et al., 2017).

3 Results and discussion

3.1 Strong astronomically paced variability in continental dust deposition, wind-driven upwelling and productivity during the warm Pliocene and early Pleistocene

Our records show strong evidence for persistent strong astronomically paced variability in oceanic export productivity across the Plio-Pleistocene transition on the NW African margin and

in the EEA (Figures 3–5). At ODP Site 659, ln[Br/tot] values and C_{37} alkenone fluxes both show significant variability at precessional (23 kyr) and obliquity (41 kyr) frequencies (Figure 5). These same periodicities are seen in the dust flux records, with intervals of aridity in North Africa and high dust inputs to the Atlantic Ocean consistently recording higher marine export productivity (Figure 5). This tight coupling between dust fluxes and productivity along the NW African continental margin is also observed in records of the Quaternary (Adkins et al., 2006; Bradtmiller et al., 2016; Kinsley et al., 2022; Matsuzaki et al., 2011; O'Mara et al., 2024; Zhao et al., 1995), but had yet to be demonstrated in the Pliocene. Strong precessional variability is also seen in our carbon isotope data, with low $\delta^{13}C_{ruber}$ values recorded at times of high Br/tot counts, dust and C_{37} fluxes. $\delta^{18}O_{ruber}$ values and surface ocean temperatures from ODP Site 659 do not show a significant precessional signal, and instead are dominated by power in the 41-kyr obliquity band (Figure 5). Obliquity power is also seen in hydroclimate ([Al+Fe]/[Si+K+Ti]) and dust fluxes, but it is weaker than precession (Figure 5). These observations show that the impact of upwelling strength on surface ocean temperature and its imprint on $\delta^{18}O_{ruber}$ values at ODP Site 659 was minor in comparison to that of glacial-interglacially conditioned change in temperature at the higher latitude sites where these waters were sourced.

We hypothesise that the strong spectral coherence between high dust fluxes and productivity/low surface ocean $\delta^{13}C$ values (Figure 3) was driven by a combination of upwelling of nutrient-rich (^{12}C-enriched) waters and increased rain-out of mineral dust driven by strong trade winds across the NW African margin. Upwelled waters provide a source of otherwise limited macronutrients (Messié and Chavez, 2015), while increased dust export from NW Africa during both summer and winter today increases modern ocean carbon export by both ballasting (Brust et al., 2011; Fischer et al., 2016) and provision of nutrients (Schlosser et al., 2014). Strong NETW are also suggested to have driven intensified wind-driven upwelling during both cold periods and precession maxima during the late Quaternary (Bradtmiller et al., 2016; Filipsson et al., 2011; McGee et al., 2013). Our data indicate that strong upwelling-induced coupling between

wind strength and ocean productivity offshore NW Africa also operated during the warm Pliocene and early Pleistocene.

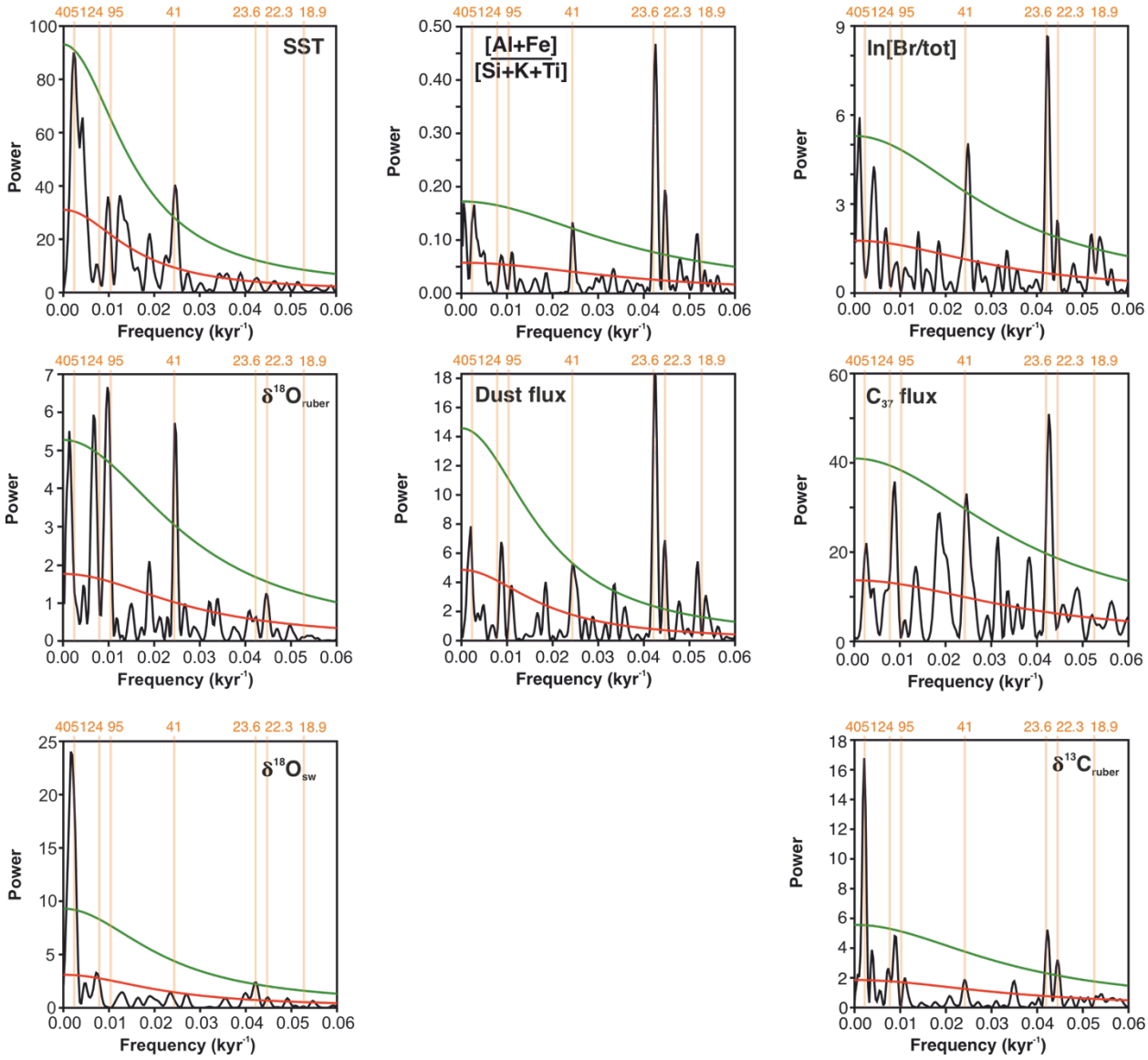

Figure 5. REDFIT spectral analysis of Site 659 records 3.5–2.2 Ma. Top row (L–R): Alkenone-derived SST, calibrated [Al+Fe]/[Si+K+Ti], ln[Br/tot] counts. Middle row: *G. ruber* (white) $\delta^{18}O$ values, median dust flux estimates, C_{37} alkenone fluxes. Bottom row: $\delta^{18}O_{sw}$ estimates, *G. ruber* (white) $\delta^{13}C$ values. Green curves mark the false-alarm level at the 95% confidence level, red curves indicate AR(1) red noise models. Orange lines and numbers indicate the frequencies equivalent to periods (in kyr) of major astronomical cycles (precession, obliquity and

eccentricity). Analyses performed and figures created using PAST software (Hammer et al., 2001).

3.2 Secular change in dust, wind-driven upwelling and productivity

3.2.1 Strengthening of the trade winds upon iNHG

An increase in the flux of terrigenous sediment during the Plio-Pleistocene transition to sites lying downwind of North Africa in the North Atlantic Ocean has been typically (but not universally; see Trauth et al. (2009)) inferred from marine sedimentary archives (deMenocal, 1995; Sarnthein et al., 1982; Tiedemann et al., 1994). Based largely on these records, it was once widely suggested that hyperaridity in North Africa (in other words, the development of a recognizable Saharan desert), originated in response to the late Pliocene intensification of Northern Hemisphere glaciation (~2.7 Ma). We now know that the Sahara is much older because geochemical records from ODP Site 659 reveal that North Africa was regularly dust-producing from at least 11 Myrs ago, persistently alternating between arid conditions like those familiar to us today and the more humid ones experienced by our mid-Holocene ancestors (Crocker et al., 2022). Nevertheless, while the astronomically paced arid-humid cycles continued, these records suggest that dry and dusty intervals intensified at roughly the same time as iNHG (Figure 1).

Early reconstructions of secular change in African hydroclimate commonly used terrigenous proportions or accumulation rates as proxies for dust fluxes with ODP Site 659, located under the centre of the North African summer dust plume, providing a landmark record of Saharan variability using this method (deMenocal, 1995; Sarnthein et al., 1982; Tiedemann et al., 1994). However, there are several complications with this approach. First, terrigenous content in marine core samples is not merely controlled by changes in terrigenous supply but also by dilution through the addition of marine sediments (chiefly $CaCO_3$ at ODP Site 659). Second, at sites proximal to continents, the terrigenous fraction consists not only of windblown dust but may also contain material transported by rivers. Third, once isolated, changes in the windblown dust fraction are governed by changes in both continental hydroclimate and wind strength. Fourth, while marine archives can provide long unbroken records of continental hydroclimate with excellent age control, these records often come with more of an attribution problem (uncertain provenance) than terrestrial archives.

To address these uncertainties at ODP Site 659, Crocker et al. (2022) used a geochemical approach, developing records of hydroclimate and grain size variability from [Al+Fe]/[Si+K+Ti] (a proxy for aeolian versus riverine inputs) and ln[Zr/Rb] (zircons concentrated in the sediment coarse fraction) respectively (Mulitza et al., 2010; Tjallingii et al., 2008). Crucially, these two ratios employ only lithophile elements, and so, unlike terrigenous fluxes, they are independent of carbonate production and seafloor dissolution. Furthermore, they also deconvolved downcore changes in terrigenous content into a dust and riverine fraction by comparing its elemental composition to the contrasting chemistry of Saharan dust and Senegal river sediments today, and fingerprinted the source of terrigenous sediments to ODP Site 659 using radiogenic isotopes (Jewell et al., 2022; Jewell et al., 2021; Kunkelova et al., 2022). These geochemical records suggest that the Pliocene-Pleistocene transition in North African climate to a more deeply arid

dusty state took a particular form. Change is recorded first in [Al+Fe]/[Si+K+Ti] which documents a shift in central tendency (~average) and dispersal (~spread) towards more arid conditions centred on ~3.1 Ma. There is widespread evidence for drying across North Africa around this time with a shift towards more arid climates recorded in the eastern Mediterranean (Grant et al., 2022; Lupien et al., 2023), and a expansion of more arid-adapted vegetation in northwest Africa (Leroy and Dupont, 1994) with a more subtle shift in East Africa (Liddy et al., 2016; Lupien et al., 2021; Yost et al., 2020).

An increase in dust fluxes and ln[Zr/Rb], both of which carry a stronger imprint of wind strength, is recorded at ODP Site 659 about 400 kyr later than the shift to a more humid climate suggested by [Al+Fe]/[Si+K+Ti]. This offset in the timing between aridification and dust fluxes suggests that increased wind strength rather than dust availability drove the increase in dust fluxes from 2.7 Ma, a hypothesis which is supported by an increase in trade wind indicator pollen species recorded offshore NW Africa (Vallé et al., 2014). The increases in dust flux and ln[Zr/Rb] are particularly noteworthy because they occur during iNHG (Figure 1) and are statistically significant (Crocker et al., 2022), unlike the inferred change in terrigenous flux (Trauth et al., 2009). The NETW dominate dust transport to the NW African margin today (Skonieczny et al., 2013) and there is no change in dust provenance at ODP Site 659 associated with the increase in dust fluxes from the Pliocene to the Pleistocene, so major shifts in regional wind patterns can also be discounted as the cause of this increase in dust flux (Crocker et al., 2022). Furthermore, terrigenous flux also increases during iNHG at EEA Sites 662 and 664, located further offshore than Site 659 (deMenocal, 1995; Ruddiman and Janecek, 1989). Although the terrigenous flux record is subject to the limitations discussed above, the shared trend at both sites strongly suggests that the NETW strengthened during iNHG. A slightly later increase in dust flux at ~2.55 Ma is recorded at ODP Site 967 in the Mediterranean Sea, however dust transport to this site is suggested to be driven by the activity of Mediteranean depressions

during late winter and spring rather than simply by the trade winds (Larrasoaña et al., 2003; Trauth et al., 2009).

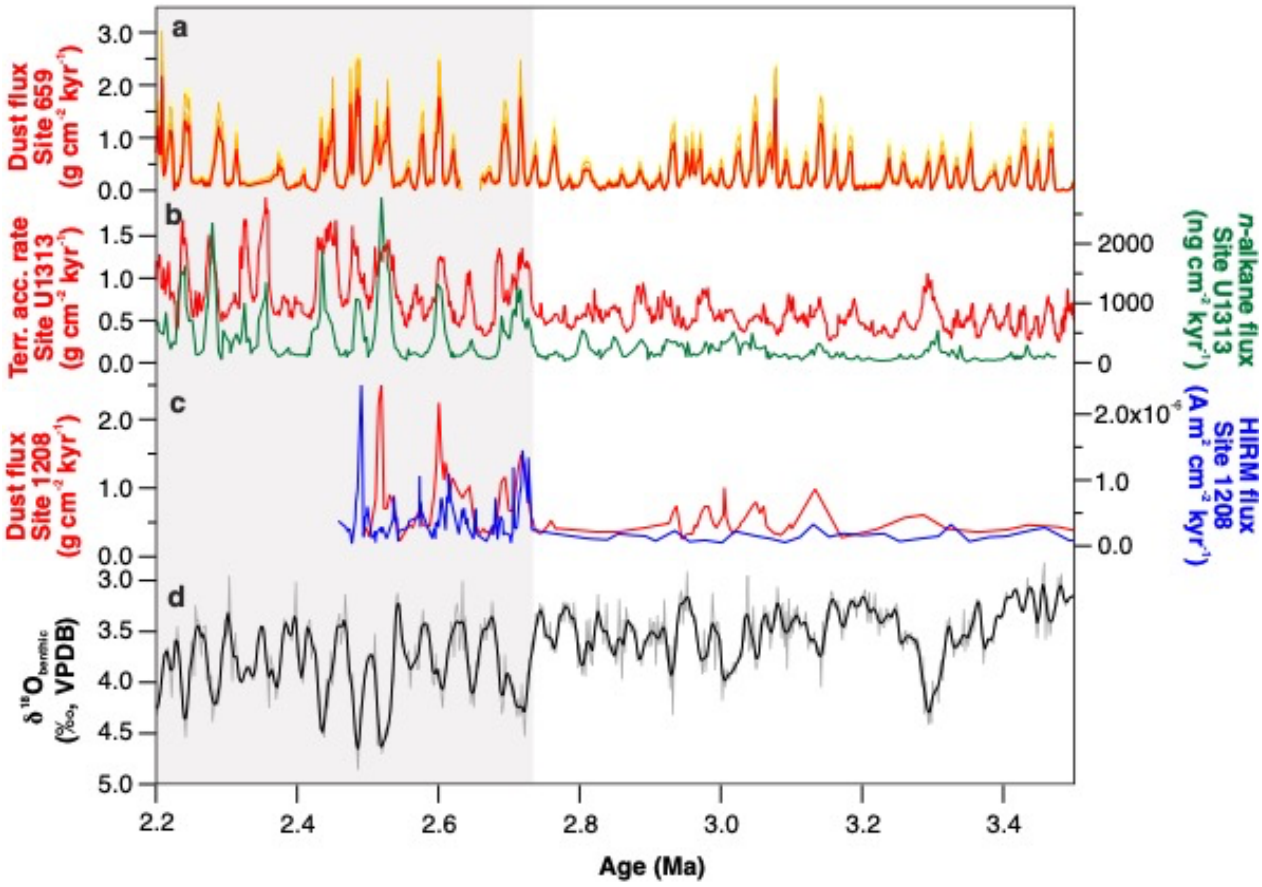

Figure 6. Dust flux variability through iNHG to mid and low latitude sites. **a** Estimated dust flux recorded at ODP Site 659 (3-point smoothed). Median value in red; 1st, 5th, 25th, 75th, 95th and 99th percentiles also shown in shades of orange/yellow (Crocker et al., 2022). **b** Dust fluxes to IODP Site U1313 in the North Atlantic (41°N), with terrigenous accumulation rates in red (Lang et al., 2014) and accumulation rates of odd-numbered long-chain *n*-alkanes in dark green (Naafs et al., 2012). **c** Dust fluxes to ODP Site 1208 in the North Pacific (36°N), with Th-derived dust fluxes in red (Abell et al., 2021) and hard isothermal remanent magnetization (HIRM) flux in blue (Bridges et al., 2023). **d** CENOGRID benthic foraminfera oxygen isotope dataset (grey line), with 20 kyr smoothing (black line) (Westerhold et al., 2020; Wilkens et al., 2017). Grey background shading indicates regime shift from 2.72 Ma.

Strengthening of the westerly wind systems during iNHG has also been proposed based on dust records from mid-latitude sites in the Pacific and Atlantic Oceans, with a sharp jump in dust fluxes reported at 2.72 Ma (Figure 6; Abell et al., 2021; Bridges et al., 2023; Lang et al., 2014; Naafs et al., 2012). The gradational increase in dust fluxes at ODP Site 659 is also centered around 2.7 Ma (Crocker et al., 2022), suggesting that the trade winds strengthened at broadly the same time as the westerlies. This implies that the effect on atmospheric circulation of

iNHG was not restricted to the mid and high latitudes (Ferrel cell) but extended deep into the (sub)tropics implying a contemporaneous invigoration of Hadley cell circulation. The jump in dust fluxes is less pronounced at ODP Site 659 than the mid-latitude sites in the path of the westerlies (Abell et al., 2021; Bridges et al., 2023; Lang et al., 2014; Naafs et al., 2012, Figure 6). We attribute this result to the proximity of ODP Site 659 to the world's most active dust source (North Africa, Ginoux et al. (2012)), which was already active during favourable astronomical configurations throughout the Pliocene (Crocker et al., 2022), whereas the records of the westerlies come from North Atlantic and North Pacific sites that lie a long way downwind of dust source regions (in North America and East Asia respectively) where dust activation and/or long distance transport jumped during iNHG from a lower base level.

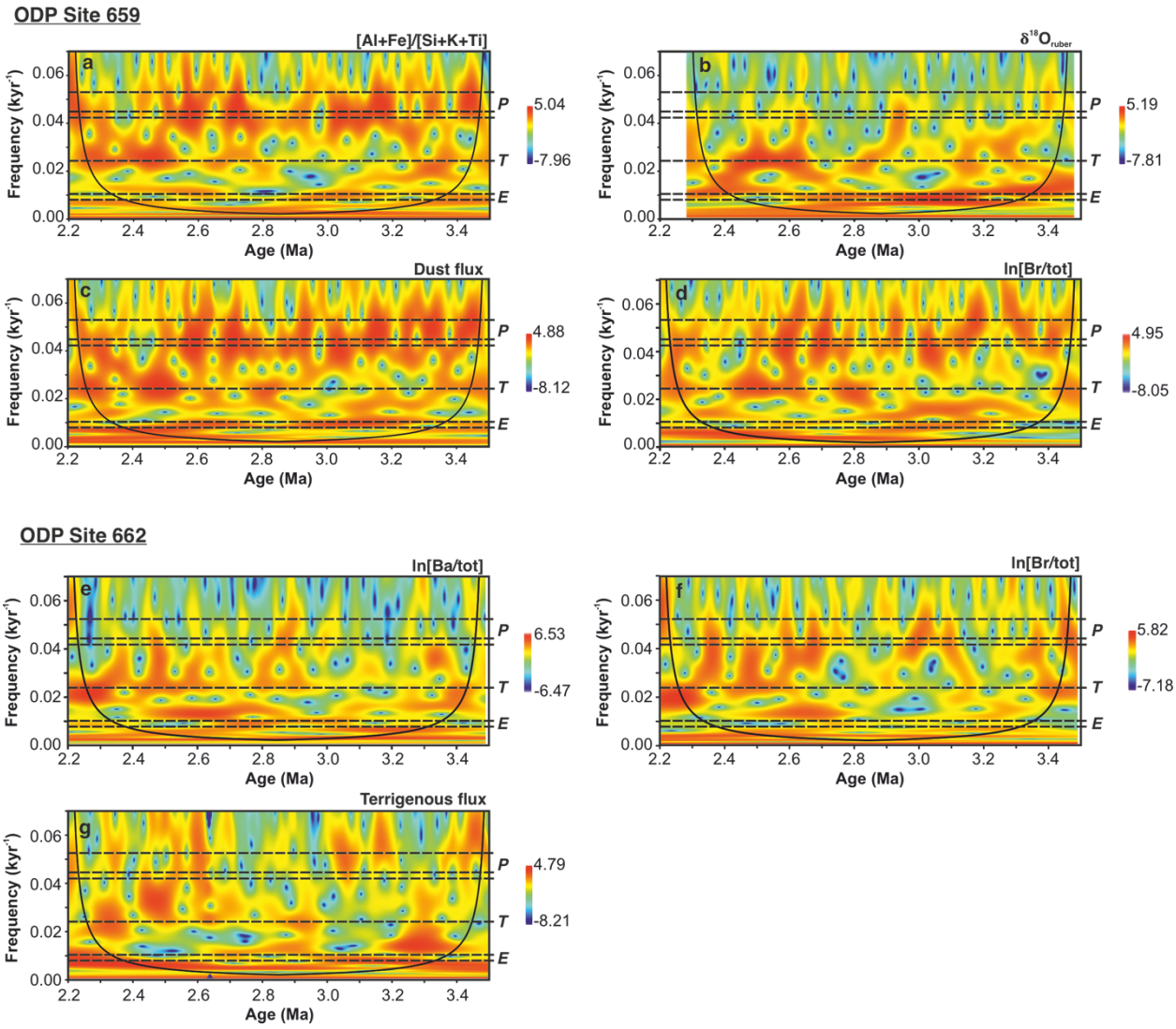

Figure 7. Wavelet analysis of eastern Tropical Atlantic data series from 3.5–2.2 Ma, **a-d** ODP Site 659: **a** Calibrated [Al+Fe]/[Si+K+Ti] values, **b** $\delta^{18}O$ of mixed layer planktonic foraminifera *G. ruber* (white), **c** Median dust flux estimates, **d** ln[Br/tot] counts measured by XRF core scanning. **e-g** ODP Site 662: **e** ln[Ba/tot] and **f** ln[Br/tot] counts measured by XRF core scanning, **g** Terrigenous flux (data from Ruddiman and Janecek (1989), with stratigraphy updated

following Herbert et al. (2010)). Horizontal dashed lines indicate frequencies of key astronomical cycles, with E = eccentricity (124 and 95 kyr), T = obliquity (also known as tilt, 41 kyr) and P = precession (23.6, 22.3 and 18.9 kyr). Analyses performed and figures created using PAST software (Hammer et al., 2001).

3.2.2 Spatial variability in the response of oceanic productivity

The intensification of northern hemisphere glaciation was accompanied by large changes in patterns of global oceanic productivity. A major shift occurred at 2.72 Ma, with the onset of strong orbitally paced pulses in productivity in parts of the equatorial and temperate Atlantic and crashes in productivity in the Southern Ocean and subarctic Pacific (Haug et al., 1999; Lawrence et al., 2013; Sigman et al., 2004). This shift in global patterns of marine productivity has been attributed to a combination of changes in wind strength/position and upper ocean stratification.

Unusually warm SST values during the Pliocene have been recorded at several sites in major mid-latitude upwelling zones, suggesting that upwelling was weaker in the Pliocene than the Pleistocene (Brierley et al., 2009; Dekens et al., 2007; Herbert and Schuffert, 1998; LaRiviere et al., 2012; Marlow et al., 2000). Multiple modelling studies show a lower intensity of upwelling-favourable winds (particularly the transient upwelling-driving wind events) under Pliocene boundary conditions (Arnold and Tziperman, 2016; Fedorov et al., 2013; Li et al., 2015; Li et al., 2019). Expanded continental wetlands during the Pliocene could also weaken upwelling strength due to localised cooling weakening alongshore upwelling-favourable winds (Fu et al., 2021). During the transition from the Pliocene to the Pleistocene, both data and model results suggest that increasing wind strength occurred in conjunction with an equatorward shift of the westerlies (e.g. Abell et al., 2021; Li et al., 2015). Another factor proposed to influence shifts in productivity between the Pliocene and Pleistocene is a shallowing of the thermocline, allowing cooler subsurface waters closer to the ocean surface (Dekens et al., 2007). Coeval shoaling of the nutricline is proposed to explain a greater availability of nutrient-rich waters at the poleward margin of the North Atlantic gyre (ODP Site 607) and in equatorial upwelling regions (ODP Site 662) (Lawrence et al., 2013). In contrast, the equatorward shift of the westerlies is suggested to have increased ocean stratification at high latitudes and caused a dramatic decline in high latitude productivity in both hemispheres, as evidenced at locations such as ODP sites 882 and 1096 (Haug et al., 1999; Sigman et al., 2004).

Astronomically paced changes in upwelling at ODP sites 659 and 662 show a very close match to variability in trade wind strength, with both sites recording increased ocean productivity (high C_{37} flux, Br/tot and Ba/tot counts) at times of high dust/terrigenous input over astronomical timescales (Figures 3–4). Both sites – but particularly ODP Site 662 – record a strengthening of the NETW upon iNHG, as well as stronger 41 kyr (obliquity) frequencies at the expense of 19 & 23 kyr (precession) in both dust/terrigenous fluxes and productivity records from 2.7–2.5 Ma (Figure 7, supplementary figure 3), suggesting an increasing high latitude influence on NETW strength. The increases in dust fluxes and inferred trade wind strength at ~2.7 Ma provoke a

jump in ocean productivity in the EEA (ODP Site 662), but not on the NW African margin (ODP Site 659).

Before 2.7 Ma, C_{37} fluxes at ODP sites 662 and 659 were similar in both magnitude and timing. After this time, peak C_{37} fluxes were approximately an order of magnitude greater at Site 662 than at Site 659 (Figure 8). This suggests that the reorganisation of the climate system in response to iNHG had a larger impact on the near-equatorial divergence-driven upwelling at ODP Site 662 than at the more northerly (18°N) ODP Site 659. However, in the modern ocean, the mechanistic forcing of upwelling (NETW strength) is broadly common to both equatorial upwelling and coastal upwelling along the NW African margin. It is unlikely, therefore, that wind strength alone can explain the differences between the two sites, and radiogenic isotope evidence suggests no large shift in the position of the wind field across iNHG (Crocker et al., 2022). It is possible that the location of ODP Site 659 distal from the zones of strongest upwelling on the NW African margin (Figure 2) makes it relatively insensitive to any changes in upwelling strength further north/closer to the coast, although over astronomical timescales, ODP Site 659 does still capture strong coupling between dust inputs and marine productivity, akin to that recorded closer in sites to the heart of the upwelling system during the Late Quaternary (e.g. Adkins et al., 2006; Bradtmiller et al., 2016).

Strengthening of the wind field can influence the supply of nutrients to the surface ocean (and hence productivity) either through increased wind-driven upwelling of nutrient rich subsurface waters or by increased delivery of nutrients via aeolian transport. An increase in the supply of iron-rich dust to the EEA could therefore boost productivity, particularly during the Pliocene when dust fluxes were low. However, both ODP sites 659 and 662 sit within a region where productivity is currently limited by nitrogen availability (with some phosphorous co-limitation) (Browning and Moore, 2023; Moore et al., 2013), hence the increased addition of iron to the surface ocean associated with the observed increase in dust fluxes would not be expected to have a strong effect on productivity at either site.

An alternative explanation for the different trends in productivity at the two sites recorded around 2.7 Ma is that the nutrient content of the upwelled waters increased at ODP Site 662 but not ODP Site 659. A major expansion of nutrient-rich southern-sourced waters into the Atlantic has been documented at 2.7 Ma (Lang et al., 2016); however, we note that the same water mass (South Atlantic Central Water) dominates the subsurface at both sites today (Peña-Izquierdo et al., 2012). Therefore, our results appear to support the hypothesis of Lawrence et al. (2013), wherein the nutricline outcrops at the surface occurring during favourable orbits from 2.7 Ma at equatorial upwelling site ODP Site 662 but not at the more northerly ODP Site 659, resulting in a much more dramatic increase in nutrient availability in the equatorial upwelling system. We that no decrease in upper ocean stratification is recorded at eastern equatorial

Atlantic ODP Site 959 (van der Weijst et al., 2022), however, like ODP Site 659, that site is dominated by coastal upwelling rather than equatorial divergence.

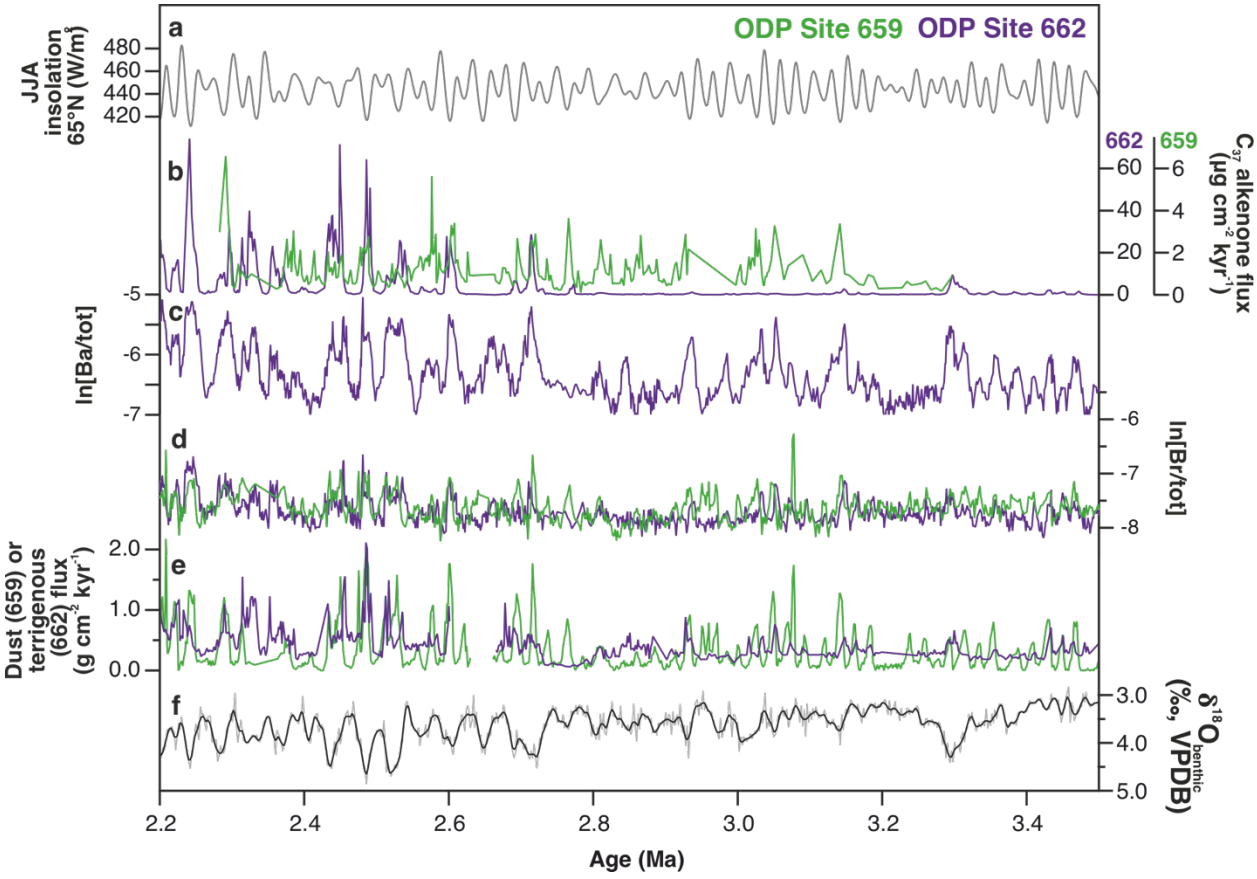

Figure 8. Comparison of Late Pliocene-early Pleistonce reconstructions of productivity at ODP sites 659 (green) and 662 (purple). **a** Summer (June, July & August) insolation at 65°N (La2004 solution) in grey (Laskar et al., 2004). **b** Flux of C_{37} alkenones recorded at ODP Site 659 (this study) and ODP Site 662 (Lawrence et al., 2013). Note different y-axis scales for each site. **c** ln[Ba/tot] counts measured by XRF core scanning of sediments from ODP Site 662. **d** ln[Br/tot] counts measured by XRF core scanning of sediments from ODP Site 659 (green) and 662 (purple). **e** Median dust flux estimates from ODP Site 659 (Crocker et al., 2022) and terrigenous flux from ODP Site 662 (data from Ruddiman and Janecek (1989), with stratigraphy updated following Herbert et al. (2010)). Note that at ODP Site 659, the proportion of dust within the sediment was estimated using a geochemical endmember unmixing approach while the terrigenous flux at ODP Site 662 includes all non-$CaCO_3$ material. **f** CENOGRID benthic

foraminfera oxygen isotope dataset (grey line), with 20 kyr smoothing (black line) (Westerhold et al., 2020; Wilkens et al., 2017).

3.3 Mechanistic forcing of African climate rooted in changes in the North Atlantic surface ocean temperature field

Next, we examine the influence of North Atlantic SST values and latitudinal gradients on North African climate, using our new records of alkenone-derived SSTs from ODP Site 659 and compare them to SST reconstructions from ODP Site 982 (58°N, Lawrence et al., 2009), IODP Site U1313 (41°N, Naafs et al., 2012; Naafs et al., 2010), ODP Site 607 (41°N, Lawrence et al., 2010) and ODP Site 662 (1°S, Herbert et al., 2010) (Figure 9).

Late Pliocene cooling in the North Atlantic Ocean is much more pronounced at higher versus lower latitudes. Strong and sustained cooling of >4°C is documented at ODP Site 982 from 3.5–2.5 Ma (Kaboth-Bahr and Mudelsee, 2022; Lawrence et al., 2009, Figure 9), while SST cooling of ~3°C is recorded at mid-latitude Atlantic sites U1313 and 607 from ~3.1 Ma, attributed to a weakening of the North Atlantic Current and southward expansion of the Arctic front (Lawrence et al., 2010; Naafs et al., 2010). In contrast, SSTs at low latitude Atlantic sites ODP sites 659 and 662 are generally warm and stable before 2.7 Ma. ODP Site 659 shows average SSTs of 25.5–27°C (with the exception of an interval of cooler temperatures of ~24.5°C at 2.93 Ma during MIS G16), with almost identical temperatures recorded in the EEA upwelling belt at ODP Site 662 (Figure 9). These results reveal that the cooling of the surface waters along the NW African margin and/or the EEA did not contribute to the intensification of arid dusty intervals on North Africa around 3.1 Ma. Instead, the recorded shift to increasingly arid conditions shown by [Al+Fe]/[Si+K+Ti] at ODP Site 659 is more closely associated with cooling of the surface ocean at higher latitudes (Figure 9). Our findings therefore point to a mechanistic

forcing mechanism rooted in the sensitivity of the tropical rainbelt to high latitude cooling and/or latitudinal temperature gradients in the North Atlantic Ocean.

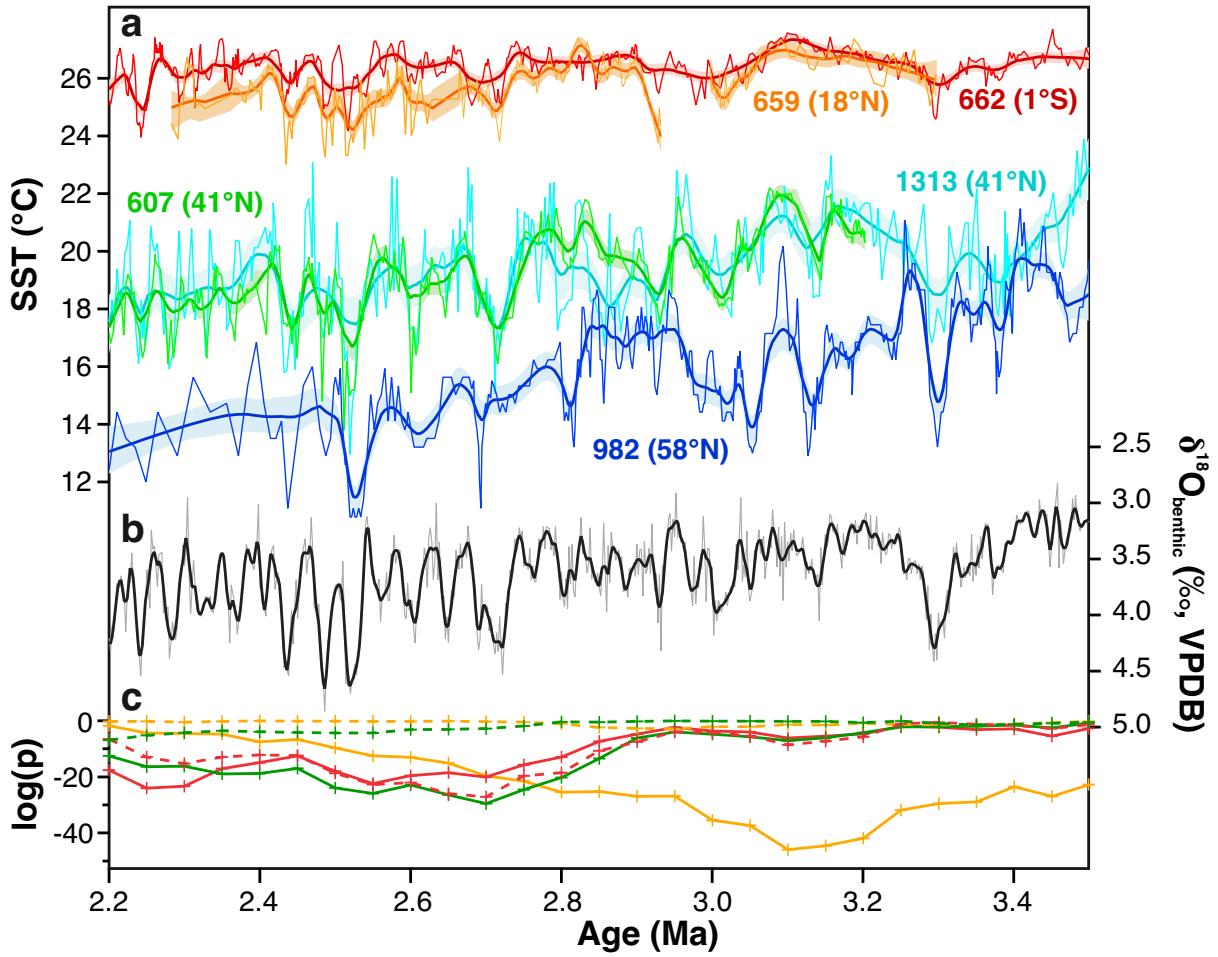

Figure 9. Evolution of North Atlantic SST from 3.5–2.2 Ma. **a** Alkenone-derived SST estimates from ODP Site 659 (orange, this study) compared to data from ODP Site 662 (red, Herbert et al., 2010), IODP Site U1313 (green, Naafs et al., 2012; Naafs et al., 2010), ODP Site 607 (pale blue, Lawrence et al., 2010) and ODP Site 982 (dark blue, Lawrence et al., 2009). Dark lines mark LOESS smoothed fits (Cleveland, 1979), with shading indicating 95% confidence interval. **b** CENOGRID benthic foraminfera oxygen isotope dataset (pale grey), with 20 kyr smoothing in black (Westerhold et al., 2020; Wilkens et al., 2017). **c** log(*p*) values indicating probability of shifts in central tendency (Mann-Whitney-Wilcoxon test , solid lines) and dispersion (Ansari-Bradley test, dashed lines) (Crocker et al., 2022). Colours indicate the analysed proxy data series, with [Al+Fe]/[Si+K+Ti] in orange, ln[Zr/Rb] in green and median dust flux in red (full datasets shown in Figure 1).

Model simulations suggest that warm temperatures in the high latitudes and weak latitudinal temperature gradients were key factors in driving a strong West African monsoon

during the warm Pliocene (Brierley and Fedorov, 2010; Burls and Fedorov, 2017; Han et al., 2023), with a strong link between latitudinal temperature gradients and African hydroclimate also invoked in the Late Miocene (Herbert et al., 2016). Pronounced high latitude cooling in the northern hemisphere from the Pliocene into the Pleistocene is also suggested to have led to a decrease in the cross-equatorial temperature gradient, shifting the ITCZ southwards and weakening the West African monsoon (Brierley and Fedorov, 2010; Wycech et al., 2022). In addition, cooling of the North Atlantic Ocean has been linked to tropospheric cooling, which reduces evapotranspiration and cloudiness and strengthens the easterly midtropospheric jet which exports moisture from the continent to the ocean, both mechanisms acting to reduce precipitation over North Africa (Liu et al., 2014; Mulitza et al., 2008). The exact role of SST-atmosphere feedbacks is one of the largest sources of uncertainty in regional precipitation predictions for the coming decades (Monerie et al., 2023; Zhang et al., 2023; Zhang and Li, 2022), with changes in both high latitude and low latitude ocean temperatures invoked to explain recent variability in Sahelian rainfall intensity (e.g. He et al., 2018; Liu et al., 2014; Monerie et al., 2019). The absence of cooling recorded at either ODP Site 659 or 662 associated with aridification in North Africa at ~3.1 Ma suggests that cooling at mid/high latitudes exerted a stronger influence over precipitation than low latitude temperatures during the warm Pliocene, a result which may have consequences for future precipitation trends if similar mechanisms apply over the coming centuries, given Arctic amplification of recent global warming.

The increase in dust export from North Africa centered around 2.7 Ma is closely associated with surface ocean cooling at all latitudes (Figure 9) during the culmination of iNHG (Lisiecki and Raymo, 2005; McClymont et al., 2023; Meyers and Hinnov, 2010; Ruggieri, 2013). The increase in latitudinal temperature gradients and ice volume is invoked to explain a strengthening of the westerly wind systems observed in both the Pacific and Atlantic Oceans (Abell et al., 2021; Bridges et al., 2023; Lang et al., 2014). Dust flux records from ODP Site 659 strongly suggest that the NETW strengthened at broadly the same time as the westerlies, presumably in response to strengthening of Hadley cell circulation driven by increasing

latitudinal temperature gradients, particularly during glacial phases (Brierley and Fedorov, 2010; Corvec and Fletcher, 2017).

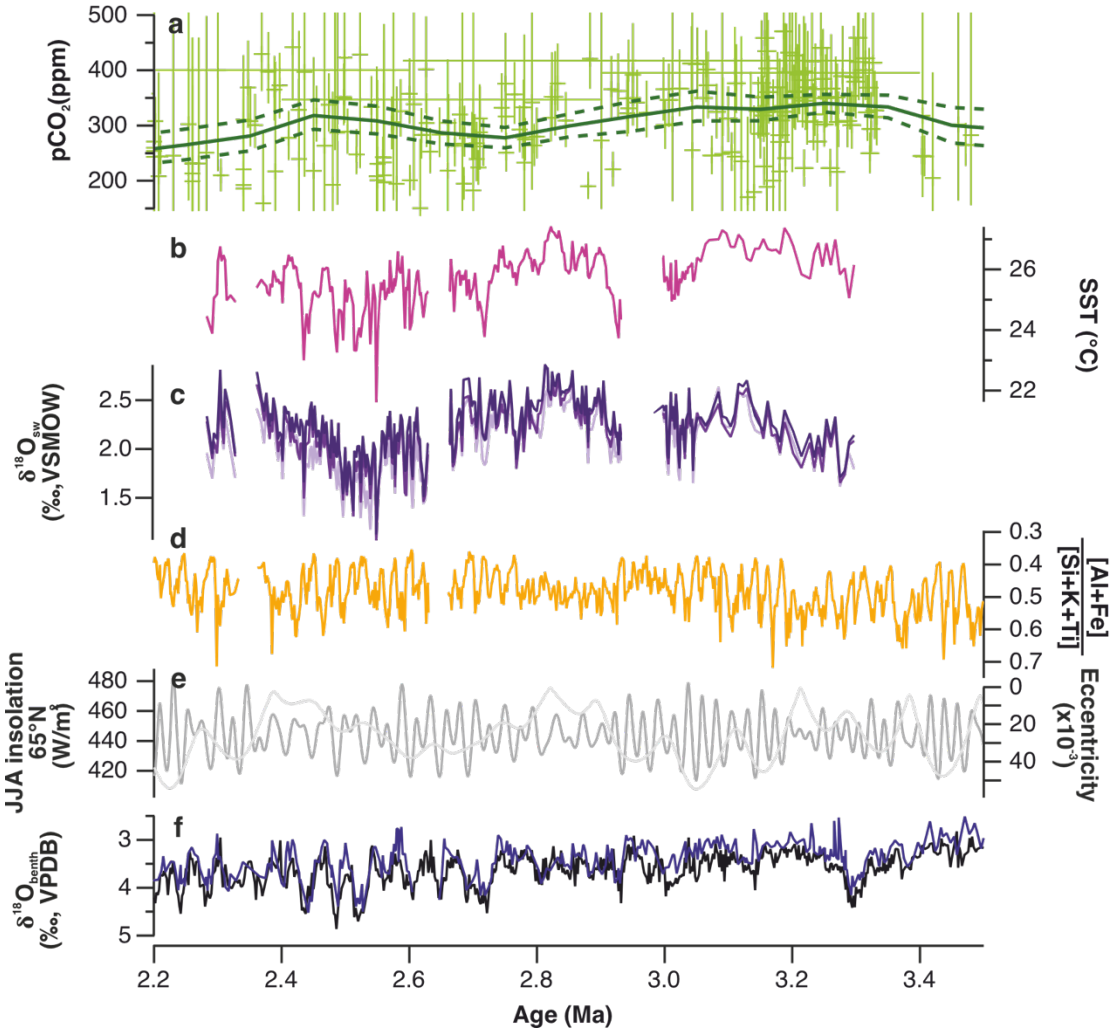

Figure 10. Late Pliocene-Early Pleistocene evolution of the tropical eastern Atlantic. **a** Reconstructed atmospheric pCO_2 values; solid line marks 100 kyr mean, dashed line indicates 95% confidence interval, individual data points in pale green (Consortium*† et al., 2023). **b** Alkenone-derived SST estimates at ODP Site 659 (pink). **c** Estimated $\delta^{18}O_{sw}$ at ODP Site 659 calculated using three different approaches to correct for global ice volume change on ocean $\delta^{18}O$, with method (1) in palest purple, method (2) in intermediate shade and method (3) in darkest purple (see section 2.3). **d** [Al+Fe]/[Si+K+Ti] of calibrated elemental abundances from ODP Site 659 (Crocker et al., 2022). **e** Orbital eccentricity (light grey) and summer (June, July & August) insolation at 65°N (La2004 solution, dark grey) (both Laskar et al., 2004). **f** ODP Site 659 benthic foraminiferal (*C. wuellerstorfi*) oxygen isotope record (dark blue line) (Tiedemann

et al., 1994 and this study) and CENOGRID benthic foraminfera oxygen isotope dataset (black) (Westerhold et al., 2020; Wilkens et al., 2017).

3.4 Sea surface salinity change documents ocean-atmosphere feedbacks

Combining our alkenone-derived SST estimates with the oxygen isotope signatures of mixed layer dwelling foraminiferal species, *G. ruber* and estimates of past sea level/global ice volume allows us to remove the imprint of both temperature and changes in the global ocean $\delta^{18}O$ on foraminiferal calcite (see section 2.3), and hence estimate past variability of the local $\delta^{18}O_{sw}$ of the upper ocean, which has a strong correlation with salinity (Bigg and Rohling, 2000; Voelker et al., 2015). The resulting local surface seawater oxygen isotope values ($\delta^{18}O_{sw}$) show a strong 400 kyr eccentricity signature (Figure 5), possibly due to the modulating influence of eccentricity over precessional forcing of the West African monsoon (Crocker et al., 2022; Kuechler et al., 2018), although local SST values also appear to contain some 400 kyr periodicity, although it is not significant at the 95% confidence level (Figure 5). From 3.3 to 2.85 Ma, our records show a shift towards higher $\delta^{18}O_{sw}$ values implying higher salinity, that appears only a partial match to the trend in eccentricity forcing (Figure 10). Taken together with the aridification signal in our XRF records (a decrease in [Al+Fe]/[Si+K+Ti]), one interpretation of the inferred salinification of surface waters along the NW African margin is that it was driven by a relative increase in evaporation over precipitation. Shifts in the location of the tropical rainbelt have been shown to not only drive precipitation changes over land, but also lead to regional ocean salinity anomalies (Vellinga and Wu, 2004).

From 2.85 to 2.5 Ma, this trend of increasing ocean salinity reverses, with a ~1‰ decrease in $\delta^{18}O_{sw}$ values suggesting decreasing surface ocean salinity despite the increase in dust fluxes at this time (Figure 10). We consider two alternative explanations of this signal. Arguably the simplest is that enhanced regional upwelling drove the freshening of surface waters offshore NW Africa (see section 3.2). Alternatively, the signal may be explained by a shift in the locus of precipitation from the land to the ocean. Many simulations of future climate change reveal a sharp contrast in precipitation trends over land and ocean, with drying in subtropical regions as proposed by the "dry gets drier" paradigm predicted over the ocean rather than over land (He and Soden, 2017). In the models, this response is traced to an increase in the land-sea temperature contrast resulting from increasing pCO_2, which strengthens subsidence over the subtropical oceans while weakening it over land, resulting in drying over the oceans but little change over the continents where precipitation increases are largely balanced by an increase in evaporation (He and Soden, 2017). Thus, a weakening of the strong land-ocean temperature contrasts which maintained a strong Pliocene West African monsoon (Berntell et al., 2021) may have led to a shift in the locus of precipitation from land to ocean, driving the decrease in surface ocean salinity recorded at ODP Site 659 from ~2.85 Ma. A recent compilation of pCO_2 estimates (Consortium*† et al., 2023) does not show a decrease in atmospheric CO_2 associated with the

decrease in $\delta^{18}O_{sw}$, but the large range in pCO_2 estimates means that an influence of this mechanism cannot be ruled out (Figure 10).

4 Conclusions

We present new records of sea surface temperature, planktonic foraminiferal stable isotopes and export productivity from the eastern tropical Atlantic (ODP sites 659 and 662), spanning the warm Pliocene to early Pleistocene, and compare them to detailed records of hydroclimate variability and dust export from North Africa. Our records reveal that the tight coupling between wind strength, dust deposition and export productivity identified over astronomical time scales in the Late Quaternary also applied during the warm Pliocene.

We find that the trade winds blowing from Africa across the (sub)tropical North Atlantic Ocean strengthened around 2.7 Ma, at a time of cooling in both the high and low latitude Atlantic Ocean. North Africa aridified earlier (from ~3.1 Ma), well before sea surface temperature cooling is documented at low latitudes. These findings highlight the importance of high latitude influences in modulating precipitation on North Africa. The increase in trade wind strength that we document around 2.7 Ma occurred in close association with a strengthening of the westerly winds and led to a contrasting response in export productivity between our two study sites, with a sharp increase in productivity documented in the eastern equatorial Atlantic but little change on the NW African margin. Our results point to invigoration of large-scale atmospheric circulation globally as glacial periods intensified during the late Pliocene and early Pleistocene.

Acknowledgments

This research was funded through the Royal Society Challenge Grant CHG\R1\170054 (PAW) and Wolfson Merit Award WM140011 (PAW). Additional funding came from University of Southampton's GCRF strategic development fund grant 519016 (PAW and AJC), a Natural Environment Research Council studentship (grant number NE/L002531/1) to AMJ. BAM was funded by an NSF Graduate Research Fellowship (grant # DGE-1144087). UR and TW were supported by the Deutsche Forschungsgemeinschaft (DFG, German Research Foundation) under Germany´s Excellence Strategy – EXC-2077 – 390741603. TDH was funded by NSF grants OCE-1459280 and OCE-1545859. This research used samples provided by (I)ODP, which was sponsored by the US National Science Foundation and participating countries under management of Joint Oceanographic Institutions, Inc. We thank Holger Kuhlman, Alexis Wülbers and Walter Hale of the Bremen Core Repository for help with sampling, Nicola Kirby and Mairin Williams for assistance with stable isotope sample preparation, Frida Simpson for assistance with TOC sample preparation and Vera Lukies for support in XRF core scanning. We thank Mark Moore, Peter Hopcroft and Florent Fayolle for discussions that helped to improve this manuscript.

Open Research

All new data presented in this study are available in the Zenodo repository (Crocker et al., 2024) under a Creative Commons Attribution 4.0 International licence.

References

Abell, J.T., Winckler, G., Anderson, R.F., Herbert, T.D., 2021. Poleward and weakened westerlies during Pliocene warmth. Nature 589, 70-75.

Adkins, J., deMenocal, P., Eshel, G., 2006. The "African humid period" and the record of marine upwelling from excess 230Th in Ocean Drilling Program Hole 658C. Paleoceanography 21, PA4203.

Akinsanola, A.A., Zhou, W., 2019. Projection of West African summer monsoon rainfall in dynamically downscaled CMIP5 models. Climate Dynamics 53, 81-95.

Ali, A., Lebel, T., 2009. The Sahelian standardized rainfall index revisited. International Journal of Climatology 29, 1705-1714.

Arndt, S., Jørgensen, B.B., LaRowe, D.E., Middelburg, J.J., Pancost, R.D., Regnier, P., 2013. Quantifying the degradation of organic matter in marine sediments: A review and synthesis. Earth-Science Reviews 123, 53-86.

Arnold, N.P., Tziperman, E.C.P.A., 2016. Reductions in midlatitude upwelling-favorable winds implied by weaker large-scale Pliocene SST gradients. Paleoceanography, n/a-n/a.

Bakun, A., 1990. Global Climate Change and Intensification of Coastal Ocean Upwelling. Science 247, 198-201.

Berends, C.J., de Boer, B., van de Wal, R.S.W., 2021. Reconstructing the evolution of ice sheets, sea level, and atmospheric CO2 during the past 3.6 million years. Clim. Past 17, 361-377.

Berntell, E., Zhang, Q., Chafik, L., Körnich, H., 2018. Representation of Multidecadal Sahel Rainfall Variability in 20th Century Reanalyses. Scientific Reports 8, 10937.

Berntell, E., Zhang, Q., Li, Q., Haywood, A.M., Tindall, J.C., Hunter, S.J., Zhang, Z., Li, X., Guo, C., Nisancioglu, K.H., Stepanek, C., Lohmann, G., Sohl, L.E., Chandler, M.A., Tan, N., Contoux, C., Ramstein, G., Baatsen, M.L.J., von der Heydt, A.S., Chandan, D., Peltier, W.R., Abe-Ouchi, A., Chan, W.L., Kamae, Y., Williams, C.J.R., Lunt, D.J., Feng, R., Otto-Bliesner, B.L., Brady, E.C., 2021. Mid-Pliocene West African Monsoon rainfall as simulated in the PlioMIP2 ensemble. Clim. Past 17, 1777-1794.

Bigg, G.R., Rohling, E.J., 2000. An oxygen isotope data set for marine waters. Journal of Geophysical Research: Oceans 105, 8527-8535.

Bolton, C.T., Lawrence, K.T., Gibbs, S.J., Wilson, P.A., Cleaveland, L.C., Herbert, T.D., 2010. Glacial–interglacial productivity changes recorded by alkenones and microfossils in late Pliocene eastern equatorial Pacific and Atlantic upwelling zones. Earth and Planetary Science Letters 295, 401-411.

Bosmans, J.H.C., Hilgen, F.J., Tuenter, E., Lourens, L.J., 2015. Obliquity forcing of low-latitude climate. Clim. Past 11, 1335-1346.

Bradtmiller, L.I., McGee, D., Awalt, M., Evers, J., Yerxa, H., Kinsley, C.W., deMenocal, P.B., 2016. Changes in biological productivity along the northwest African margin over the past 20,000 years. Paleoceanography 31, 185-202.

Bridges, J.D., Tarduno, J.A., Cottrell, R.D., Herbert, T.D., 2023. Rapid strengthening of westerlies accompanied intensification of Northern Hemisphere glaciation. Nature Communications 14, 3905.

Brierley, C.M., Fedorov, A.V., 2010. Relative importance of meridional and zonal sea surface temperature gradients for the onset of the ice ages and Pliocene-Pleistocene climate evolution. Paleoceanography 25, PA2214.

Brierley, C.M., Fedorov, A.V., Liu, Z., Herbert, T.D., Lawrence, K.T., LaRiviere, J.P., 2009. Greatly Expanded Tropical Warm Pool and Weakened Hadley Circulation in the Early Pliocene. Science 323, 1714-1718.

Brierley, C.M., Zhao, A., Harrison, S.P., Braconnot, P., Williams, C.J.R., Thornalley, D.J.R., Shi, X., Peterschmitt, J.Y., Ohgaito, R., Kaufman, D.S., Kageyama, M., Hargreaves, J.C., Erb, M.P., Emile-Geay, J., D'Agostino, R., Chandan, D., Carré, M., Bartlein, P.J., Zheng, W., Zhang, Z., Zhang, Q., Yang, H., Volodin, E.M., Tomas, R.A., Routson, C., Peltier, W.R., Otto-Bliesner, B., Morozova, P.A., McKay, N.P., Lohmann, G., Legrande, A.N., Guo, C., Cao, J., Brady, E., Annan, J.D., Abe-Ouchi, A., 2020. Large-scale features and evaluation of the PMIP4-CMIP6 midHolocene simulations. Clim. Past 16, 1847-1872.

Browning, T.J., Moore, C.M., 2023. Global analysis of ocean phytoplankton nutrient limitation reveals high prevalence of co-limitation. Nature Communications 14, 5014.

Brust, J., Schulz-Bull, D.E., Leipe, T., Chavagnac, V., Waniek, J.J., 2011. Descending particles: From the atmosphere to the deep ocean—A time series study in the subtropical NE Atlantic. Geophysical Research Letters 38, L06603.

Burls, N.J., Fedorov, A.V., 2017. Wetter subtropics in a warmer world: Contrasting past and future hydrological cycles. Proceedings of the National Academy of Sciences 114, 12888-12893.
Byrne, M.P., O'Gorman, P.A., 2015. The Response of Precipitation Minus Evapotranspiration to Climate Warming: Why the "Wet-Get-Wetter, Dry-Get-Drier" Scaling Does Not Hold over Land. Journal of Climate 28, 8078-8092.
Canfield, D.E., 1993. Organic Matter Oxidation in Marine Sediments. Springer Berlin Heidelberg, Berlin, Heidelberg, pp. 333-363.
Cleveland, W.S., 1979. Robust Locally Weighted Regression and Smoothing Scatterplots. Journal of the American Statistical Association 74, 829-836.
Collins, J.A., Govin, A., Mulitza, S., Heslop, D., Zabel, M., Hartmann, J., Roehl, U., Wefer, G., 2013. Abrupt shifts of the Sahara-Sahel boundary during Heinrich stadials. Clim. Past 9, 1181-1191.
The Cenozoic CO2 Proxy Integration Project Consortium., Hönisch, B., Royer, D.L., Breecker, D.O., Polissar, P.J., Bowen, G.J., Henehan, M.J., Cui, Y., Steinthorsdottir, M., McElwain, J.C., Kohn, M.J., Pearson, A., Phelps, S.R., Uno, K.T., Ridgwell, A., Anagnostou, E., Austermann, J., Badger, M.P.S., Barclay, R.S., Bijl, P.K., Chalk, T.B., Scotese, C.R., de la Vega, E., DeConto, R.M., Dyez, K.A., Ferrini, V., Franks, P.J., Giulivi, C.F., Gutjahr, M., Harper, D.T., Haynes, L.L., Huber, M., Snell, K.E., Keisling, B.A., Konrad, W., Lowenstein, T.K., Malinverno, A., Guillermic, M., Mejía, L.M., Milligan, J.N., Morton, J.J., Nordt, L., Whiteford, R., Roth-Nebelsick, A., Rugenstein, J.K.C., Schaller, M.F., Sheldon, N.D., Sosdian, S., Wilkes, E.B., Witkowski, C.R., Zhang, Y.G., Anderson, L., Beerling, D.J., Bolton, C., Cerling, T.E., Cotton, J.M., Da, J., Ekart, D.D., Foster, G.L., Greenwood, D.R., Hyland, E.G., Jagniecki, E.A., Jasper, J.P., Kowalczyk, J.B., Kunzmann, L., Kürschner, W.M., Lawrence, C.E., Lear, C.H., Martínez-Botí, M.A., Maxbauer, D.P., Montagna, P., Naafs, B.D.A., Rae, J.W.B., Raitzsch, M., Retallack, G.J., Ring, S.J., Seki, O., Sepúlveda, J., Sinha, A., Tesfamichael, T.F., Tripati, A., van der Burgh, J., Yu, J., Zachos, J.C., Zhang, L., 2023. Toward a Cenozoic history of atmospheric CO_2. Science 382, eadi5177.
Coplen, T.B., 1988. Normalization of oxygen and hydrogen isotope data. Chemical Geology: Isotope Geoscience section 72, 293-297.
Corvec, S., Fletcher, C.G., 2017. Changes to the tropical circulation in the mid-Pliocene and their implications for future climate. Climate of the Past 13, 135-147.
Crocker, A.J., Jewell, A.M., Mitsunaga, B., Buchanan, S., Brombacher, A., Hambach, B., Wilding, M.R., Westerhold, T., Röhl, U., Russell, J.M., Herbert, T.D., Xuan, C., Wilson, P.A., 2024. Dataset: Increased North African dust fluxes and higher productivity in the Eastern Equatorial Atlantic Ocean linked to stronger trade winds from about 2.7 million years ago [Dataset]. In Paleoceanography and Paleoclimatology. Zenodo. https://doi.org/10.5281/zenodo.10650361.
Crocker, A.J., Naafs, B.D.A., Westerhold, T., James, R.H., Cooper, M.J., Röhl, U., Pancost, R.D., Xuan, C., Osborne, C.P., Beerling, D.J., Wilson, P.A., 2022. Astronomically controlled aridity in the Sahara since at least 11 million years ago. Nature Geoscience 15, 671-676.
Cropper, T.E., Hanna, E., Bigg, G.R., 2014. Spatial and temporal seasonal trends in coastal upwelling off Northwest Africa, 1981–2012. Deep Sea Research Part I: Oceanographic Research Papers 86, 94-111.
Curry, W.B., Thunell, R.C., Honjo, S., 1983. Seasonal changes in the isotopic composition of planktonic foraminifera collected in Panama Basin sediment traps. Earth and Planetary Science Letters 64, 33-43.
d'Orbigny, A.D., 1839. Foraminiferes, in: de la Sagra, R. (Ed.), Histoire physique, politique et naturelle de l'ile de Cuba: Ornithologie de l'ile de Cuba. Bertrand, Paris, France pp. 1-224.
de la Vega, E., Chalk, T.B., Wilson, P.A., Bysani, R.P., Foster, G.L., 2020. Atmospheric CO2 during the Mid-Piacenzian Warm Period and the M2 glaciation. Scientific Reports 10, 11002.
Dekens, P.S., Ravelo, A.C., McCarthy, M.D., 2007. Warm upwelling regions in the Pliocene warm period. Paleoceanography 22, PA3211.
deMenocal, P.B., 1995. Plio-Pleistocene African Climate. Science 270, 53-59.
Dillon, J.T., Huang, Y., 2015. TEXPRESS v1.0: A MATLAB toolbox for efficient processing of GDGT LC–MS data. Organic Geochemistry 79, 44-48.
Drake, N.A., Blench, R.M., Armitage, S.J., Bristow, C.S., White, K.H., 2011. Ancient watercourses and biogeography of the Sahara explain the peopling of the desert. Proceedings of the National Academy of Sciences 108, 458-462.
Dymond, J., Suess, E., Lyle, M., 1992. Barium in Deep-Sea Sediment: A Geochemical Proxy for Paleoproductivity. Paleoceanography 7, 163-181.
Ehrmann, W., Schmiedl, G., 2021. Nature and dynamics of North African humid and dry periods during the last 200,000 years documented in the clay fraction of Eastern Mediterranean deep-sea sediments. Quaternary Science Reviews 260, 106925.

Esri, D., GeoEye, i-cubed, USDA FSA, USGS, AEX, Getmapping, Aerogrid, IGN, IGP, swisstopo, and the GIS User Community, 2023. ESRI World Imagery.
Fairbanks, R.G., 1989. A 17,000-year glacio-eustatic sea level record: influence of glacial melting rates on the Younger Dryas event and deep-ocean circulation. Nature 342, 637-642.
Fedorov, A.V., Brierley, C.M., Lawrence, K.T., Liu, Z., Dekens, P.S., Ravelo, A.C., 2013. Patterns and mechanisms of early Pliocene warmth. Nature 496, 43-49.
Feng, R., Bhattacharya, T., Otto-Bliesner, B.L., Brady, E.C., Haywood, A.M., Tindall, J.C., Hunter, S.J., Abe-Ouchi, A., Chan, W.-L., Kageyama, M., Contoux, C., Guo, C., Li, X., Lohmann, G., Stepanek, C., Tan, N., Zhang, Q., Zhang, Z., Han, Z., Williams, C.J.R., Lunt, D.J., Dowsett, H.J., Chandan, D., Peltier, W.R., 2022. Past terrestrial hydroclimate sensitivity controlled by Earth system feedbacks. Nature Communications 13, 1306.
Filipsson, H.L., Romero, O.E., Stuut, J.-B.W., Donner, B., 2011. Relationships between primary productivity and bottom-water oxygenation off northwest Africa during the last deglaciation. Journal of Quaternary Science 26, 448-456.
Fischer, G., Romero, O., Merkel, U., Donner, B., Iversen, M., Nowald, N., Ratmeyer, V., Ruhland, G., Klann, M., Wefer, G., 2016. Deep ocean mass fluxes in the coastal upwelling off Mauritania from 1988 to 2012: variability on seasonal to decadal timescales. Biogeosciences 13, 3071-3090.
Fu, M., Cane, M.A., Molnar, P., Tziperman, E., 2021. Wetter Subtropics Lead to Reduced Pliocene Coastal Upwelling. Paleoceanography and Paleoclimatology 36, e2021PA004243.
Ganssen, G.M., Kroon, D., 2000. The isotopic signature of planktonic foraminifera from NE Atlantic surface sediments: implications for the reconstruction of past oceanic conditions. Journal of the Geological Society 157, 693-699.
Giannini, A., Kaplan, A., 2019. The role of aerosols and greenhouse gases in Sahel drought and recovery. Climatic Change 152, 449-466.
Ginoux, P., Prospero, J.M., Gill, T.E., Hsu, N.C., Zhao, M., 2012. Global-scale attribution of anthropogenic and natural dust sources and their emission rates based on MODIS Deep Blue aerosol products. Reviews of Geophysics 50, RG3005.
Gorelick, N., Hancher, M., Dixon, M., Ilyushchenko, S., Thau, D., Moore, R., 2017. Google Earth Engine: Planetary-scale geospatial analysis for everyone. Remote Sensing of Environment 202, 18-27.
Grant, K.M., Amarathunga, U., Amies, J.D., Hu, P., Qian, Y., Penny, T., Rodriguez-Sanz, L., Zhao, X., Heslop, D., Liebrand, D., Hennekam, R., Westerhold, T., Gilmore, S., Lourens, L.J., Roberts, A.P., Rohling, E.J., 2022. Organic carbon burial in Mediterranean sapropels intensified during Green Sahara Periods since 3.2 Myr ago. Communications Earth & Environment 3, 11.
Grant, K.M., Rohling, E.J., Westerhold, T., Zabel, M., Heslop, D., Konijnendijk, T., Lourens, L., 2017. A 3 million year index for North African humidity/aridity and the implication of potential pan-African Humid periods. Quaternary Science Reviews 171, 100-118.
Greve, P., Orlowsky, B., Mueller, B., Sheffield, J., Reichstein, M., Seneviratne, S.I., 2014. Global assessment of trends in wetting and drying over land. Nature Geosci 7, 716–721.
Grimalt, J.O., Rullkötter, J., Sicre, M.-A., Summons, R., Farrington, J., Harvey, H.R., Goñi, M., Sawada, K., 2000. Modifications of the C37 alkenone and alkenoate composition in the water column and sediment: Possible implications for sea surface temperature estimates in paleoceanography. Geochemistry, Geophysics, Geosystems 1.
Hagen, E., Schemainda, R., 1987. On the zonal distribution of South Atlantic Central Water (SACW) along a section off Cape Blanc, Northwest Africa. Oceanologica Acta, Special issue Proceedings International Symposium on Equatorial Vertical Motion, Paris, 6-10 May 1985, 61-70.
Hagos, S.M., Cook, K.H., 2008. Ocean Warming and Late-Twentieth-Century Sahel Drought and Recovery. Journal of Climate 21, 3797-3814.
Hammer, Ø., Harper, D.A.T., Ryan, P.D., 2001. PAST: Paleontological Statistics Software Package for Education and Data Analysis. Palaeontologia Electronica 4, 9.
Han, Z., Li, G., Zhang, Q., 2023. Changes in Sahel summer rainfall in a global warming climate: contrasting the mid-Pliocene and future regional hydrological cycles. Climate Dynamics 61, 1353-1370.
Haug, G.H., Sigman, D.M., Tiedemann, R., Pedersen, T.F., Sarnthein, M., 1999. Onset of permanent stratification in the subarctic Pacific Ocean. Nature 401, 779-782.
He, J., Johnson, N.C., Vecchi, G.A., Kirtman, B., Wittenberg, A.T., Sturm, S., 2018. Precipitation Sensitivity to Local Variations in Tropical Sea Surface Temperature. Journal of Climate 31, 9225-9238.
He, J., Soden, B.J., 2017. A re-examination of the projected subtropical precipitation decline. Nature Climate Change 7, 53-57.

Held, I.M., Soden, B.J., 2006. Robust Responses of the Hydrological Cycle to Global Warming. Journal of Climate 19, 5686-5699.
Hély, C., Lézine, A.-M., 2014. Holocene changes in African vegetation: tradeoff between climate and water availability. Climate of the Past 10, 681-686.
Herbert, T.D., 2001. Review of alkenone calibrations (culture, water column, and sediments). Geochemistry, Geophysics, Geosystems 2.
Herbert, T.D., Lawrence, K.T., Tzanova, A., Peterson, L.C., Caballero-Gill, R., Kelly, C.S., 2016. Late Miocene global cooling and the rise of modern ecosystems. Nature Geosci 9, 843-847.
Herbert, T.D., Peterson, L.C., Lawrence, K.T., Liu, Z., 2010. Tropical Ocean Temperatures Over the Past 3.5 Million Years. Science 328, 1530-1534.
Herbert, T.D., Schuffert, J.D., 1998. Alkenone unsaturation estimates of late Miocene through late Pliocene sea-surface temperatures at Site 958. Proc. Ocean Drill. Program Sci. Results, 159T, 17-21.
Hilgen, F.J., Krijgsman, W., Langereis, C.G., Lourens, L.J., Santarelli, A., Zachariasse, W.J., 1995. Extending the astronomical (polarity) time scale into the Miocene. Earth and Planetary Science Letters 136, 495-510.
Hopcroft, P.O., Valdes, P.J., 2021. Paleoclimate-conditioning reveals a North Africa land–atmosphere tipping point. Proceedings of the National Academy of Sciences 118, e2108783118.
Hut, G., 1987. Consultants' group meeting on stable isotope reference samples for geochemical and hydrological investigations, Consultants' group meeting on stable isotope reference samples for geochemical and hydrological investigations, International Atomic Energy Agency (IAEA).
Jentzen, A., Schönfeld, J., Schiebel, R., 2018. Assessment of the Effect of Increasing Temperature On the Ecology and Assemblage Structure of Modern Planktic Foraminifers in the Caribbean and Surrounding Seas. Journal of Foraminiferal Research 48, 251-272.
Jewell, A.M., Cooper, M.J., Milton, J.A., James, R.H., Crocker, A.J., Wilson, P.A., 2022. Chemical isolation and isotopic analysis of terrigenous sediments with emphasis on effective removal of contaminating marine phases including barite. Chemical Geology 589, 120673.
Jewell, A.M., Drake, N., Crocker, A.J., Bakker, N.L., Kunkelova, T., Bristow, C.S., Cooper, M.J., Milton, J.A., Breeze, P.S., Wilson, P.A., 2021. Three North African dust source areas and their geochemical fingerprint. Earth and Planetary Science Letters 554, 116645.
Johns, W.E., Brandt, P., Bourlès, B., Tantet, A., Papapostolou, A., Houk, A., 2014. Zonal structure and seasonal variability of the Atlantic Equatorial Undercurrent. Climate Dynamics 43, 3047-3069.
Jonkers, L., Kučera, M., 2015. Global analysis of seasonality in the shell flux of extant planktonic Foraminifera. Biogeosciences 12, 2207-2226.
Kaboth-Bahr, S., Mudelsee, M., 2022. The multifaceted history of the Walker Circulation during the Plio-Pleistocene. Quaternary Science Reviews 286, 107529.
Karas, C., Nürnberg, D., Gupta, A.K., Tiedemann, R., Mohan, K., Bickert, T., 2009. Mid-Pliocene climate change amplified by a switch in Indonesian subsurface throughflow. Nature Geoscience 2, 434-438.
Kinsley, C.W., Bradtmiller, L.I., McGee, D., Galgay, M., Stuut, J.-B., Tjallingii, R., Winckler, G., deMenocal, P.B., 2022. Orbital- and Millennial-Scale Variability in Northwest African Dust Emissions Over the Past 67,000 years. Paleoceanography and Paleoclimatology 36, e2020PA004137.
Kok, J.F., Adebiyi, A.A., Albani, S., Balkanski, Y., Checa-Garcia, R., Chin, M., Colarco, P.R., Hamilton, D.S., Huang, Y., Ito, A., Klose, M., Li, L., Mahowald, N.M., Miller, R.L., Obiso, V., Pérez García-Pando, C., Rocha-Lima, A., Wan, J.S., 2021. Contribution of the world's main dust source regions to the global cycle of desert dust. Atmos. Chem. Phys. 21, 8169-8193.
Kuechler, R.R., Dupont, L.M., Schefuß, E., 2018. Hybrid insolation forcing of Pliocene monsoon dynamics in West Africa. Climate of the Past 14, 73-84.
Kuechler, R.R., Schefuß, E., Beckmann, B., Dupont, L., Wefer, G., 2013. NW African hydrology and vegetation during the Last Glacial cycle reflected in plant-wax-specific hydrogen and carbon isotopes. Quaternary Science Reviews 82, 56-67.
Kunkelova, T., Crocker, A.J., Jewell, A.M., Breeze, P.S., Drake, N.A., Cooper, M.J., Milton, J.A., Hennen, M., Shahgedanova, M., Petraglia, M., Wilson, P.A., 2022. Dust sources in Westernmost Asia are geochemically distinct from those of the Eastern Sahara. Quaternary Science Reviews 294, 107717.
Kurihara, Y., 2020. GCOM-C/SGLI Sea Surface Temperature (SST) ATBD.
Lang, D.C., Bailey, I., Wilson, P.A., Beer, C.J., Bolton, C.T., Friedrich, O., Newsam, C., Spencer, M.R., Gutjahr, M., Foster, G.L., Cooper, M.J., Milton, J.A., 2014. The transition on North America from the warm humid Pliocene to the glaciated Quaternary traced by eolian dust deposition at a benchmark North Atlantic Ocean drill site. Quaternary Science Reviews 93, 125-141.

Lang, D.C., Bailey, I., Wilson, P.A., Chalk, T.B., Foster, G.L., Gutjahr, M., 2016. Incursions of southern-sourced water into the deep North Atlantic during late Pliocene glacial intensification. Nature Geoscience 9, 375-379.
LaRiviere, J.P., Ravelo, A.C., Crimmins, A., Dekens, P.S., Ford, H.L., Lyle, M., Wara, M.W., 2012. Late Miocene decoupling of oceanic warmth and atmospheric carbon dioxide forcing. Nature 486, 97-100.
Larrasoaña, J.C., Roberts, A.P., Rohling, E.J., 2013. Dynamics of green Sahara periods and their role in hominin evolution. PloS one 8, e76514.
Larrasoaña, J.C., Roberts, A.P., Rohling, E.J., Winklhofer, M., Wehausen, R., 2003. Three million years of monsoon variability over the northern Sahara. Climate Dynamics 21, 689-698.
Laskar, J., Robutel, P., Joutel, F., Gastineau, M., Correia, A.C.M., Levrard, B., 2004. A long-term numerical solution for the insolation quantities of the Earth. Astronomy & Astrophysics 428, 261-285.
Lathuilière, C., Echevin, V., Lévy, M., 2008. Seasonal and intraseasonal surface chlorophyll-a variability along the northwest African coast. Journal of Geophysical Research: Oceans 113.
Lawrence, K.T., Herbert, T.D., Brown, C.M., Raymo, M.E., Haywood, A.M., 2009. High-amplitude variations in North Atlantic sea surface temperature during the early Pliocene warm period. Paleoceanography 24, PA2218.
Lawrence, K.T., Sigman, D.M., Herbert, T.D., Riihimaki, C.A., Bolton, C.T., Martinez-Garcia, A., Rosell-Mele, A., Haug, G.H., 2013. Time-transgressive North Atlantic productivity changes upon Northern Hemisphere glaciation. Paleoceanography 28, 740-751.
Lawrence, K.T., Sosdian, S., White, H.E., Rosenthal, Y., 2010. North Atlantic climate evolution through the Plio-Pleistocene climate transitions. Earth and Planetary Science Letters 300, 329-342.
Lázaro, C., Fernandes, M.J., Santos, A.M.P., Oliveira, P., 2005. Seasonal and interannual variability of surface circulation in the Cape Verde region from 8 years of merged T/P and ERS-2 altimeter data. Remote Sensing of Environment 98, 45-62.
Leroy, S., Dupont, L., 1994. Development of vegetation and continental aridity in northwestern Africa during the Late Pliocene: the pollen record of ODP site 658. Palaeogeography, Palaeoclimatology, Palaeoecology 109, 295-316.
Li, X., Jiang, D., Zhang, Z., Zhang, R., Tian, Z., Yan, Q., 2015. Mid-Pliocene westerlies from PlioMIP simulations. Advances in Atmospheric Sciences 32, 909-923.
Li, Z., Luo, Y., Arnold, N., Tziperman, E., 2019. Reductions in Strong Upwelling-Favorable Wind Events in the Pliocene. Paleoceanography and Paleoclimatology n/a.
Liddy, H.M., Feakins, S.J., Tierney, J.E., 2016. Cooling and drying in northeast Africa across the Pliocene. Earth and Planetary Science Letters 449, 430-438.
Lisiecki, L.E., Raymo, M.E., 2005. A Pliocene-Pleistocene stack of 57 globally distributed benthic δ18O records. Paleoceanography 20, PA1003.
Liu, Y., Chiang, J.C.H., Chou, C., Patricola, C.M., 2014. Atmospheric teleconnection mechanisms of extratropical North Atlantic SST influence on Sahel rainfall. Climate Dynamics 43, 2797-2811.
Lourens, L.J., Antonarakou, A., Hilgen, F.J., Van Hoof, A.A.M., Vergnaud-Grazzini, C., Zachariasse, W.J., 1996. Evaluation of the Plio-Pleistocene astronomical timescale. Paleoceanography 11, 391-413.
Lupien, R., Uno, K., Rose, C., deRoberts, N., Hazan, C., de Menocal, P., Polissar, P., 2023. Low-frequency orbital variations controlled climatic and environmental cycles, amplitudes, and trends in northeast Africa during the Plio-Pleistocene. Communications Earth & Environment 4, 360.
Lupien, R.L., Russell, J.M., Yost, C.L., Kingston, J.D., Deino, A.L., Logan, J., Schuh, A., Cohen, A.S., 2021. Vegetation change in the Baringo Basin, East Africa across the onset of Northern Hemisphere glaciation 3.3–2.6 Ma. Palaeogeography, Palaeoclimatology, Palaeoecology 570, 109426.
Marlow, J.R., Lange, C.B., Wefer, G., Rosell-Mel√©, A., 2000. Upwelling Intensification As Part of the Pliocene-Pleistocene Climate Transition. Science 290, 2288-2291.
Martinez-Boti, M.A., Foster, G.L., Chalk, T.B., Rohling, E.J., Sexton, P.F., Lunt, D.J., Pancost, R.D., Badger, M.P.S., Schmidt, D.N., 2015. Plio-Pleistocene climate sensitivity evaluated using high-resolution CO2 records. Nature 518, 49-54.
Martinez-Ruiz, F., Kastner, M., Paytan, A., Ortega-Huertas, M., Bernasconi, S.M., 2000. Geochemical evidence for enhanced productivity during S1 sapropel deposition in the eastern Mediterranean. Paleoceanography 15, 200-209.
Matsuzaki, K.M.R., Eynaud, F., Malaizé, B., Grousset, F.E., Tisserand, A., Rossignol, L., Charlier, K., Jullien, E., 2011. Paleoceanography of the Mauritanian margin during the last two climatic cycles: From planktonic foraminifera to African climate dynamics. Marine Micropaleontology 79, 67-79.
McClymont, E.L., Ford, H.L., Ho, S.L., Tindall, J.C., Haywood, A.M., Alonso-Garcia, M., Bailey, I., Berke, M.A., Littler, K., Patterson, M.O., Petrick, B., Peterse, F., Ravelo, A.C., Risebrobakken, B., De Schepper, S., Swann, G.E.A., Thirumalai, K., Tierney, J.E., van der Weijst, C., White, S., Abe-Ouchi, A., Baatsen, M.L.J., Brady, E.C.,

Chan, W.L., Chandan, D., Feng, R., Guo, C., von der Heydt, A.S., Hunter, S., Li, X., Lohmann, G., Nisancioglu, K.H., Otto-Bliesner, B.L., Peltier, W.R., Stepanek, C., Zhang, Z., 2020. Lessons from a high-CO2 world: an ocean view from ∼3 million years ago. Clim. Past 16, 1599-1615.
McClymont, E.L., Ho, S.L., Ford, H.L., Bailey, I., Berke, M.A., Bolton, C.T., De Schepper, S., Grant, G.R., Groeneveld, J., Inglis, G.N., Karas, C., Patterson, M.O., Swann, G.E.A., Thirumalai, K., White, S.M., Alonso-Garcia, M., Anand, P., Hoogakker, B.A.A., Littler, K., Petrick, B.F., Risebrobakken, B., Abell, J.T., Crocker, A.J., de Graaf, F., Feakins, S.J., Hargreaves, J.C., Jones, C.L., Markowska, M., Ratnayake, A.S., Stepanek, C., Tangunan, D., 2023. Climate Evolution Through the Onset and Intensification of Northern Hemisphere Glaciation. Reviews of Geophysics 61, e2022RG000793.
McGee, D., deMenocal, P.B., Winckler, G., Stuut, J.B.W., Bradtmiller, L.I., 2013. The magnitude, timing and abruptness of changes in North African dust deposition over the last 20,000 yr. Earth and Planetary Science Letters 371-372, 163-176.
Messié, M., Chavez, F.P., 2015. Seasonal regulation of primary production in eastern boundary upwelling systems. Progress in Oceanography 134, 1-18.
Meyers, S.R., Hinnov, L.A., 2010. Northern Hemisphere glaciation and the evolution of Plio-Pleistocene climate noise. Paleoceanography 25, PA3207.
Mittelstaedt, E., 1991. The ocean boundary along the northwest African coast: Circulation and oceanographic properties at the sea surface. Progress in Oceanography 26, 307-355.
Monerie, P.-A., Biasutti, M., Mignot, J., Mohino, E., Pohl, B., Zappa, G., 2023. Storylines of Sahel precipitation change: Roles of the North Atlantic and Euro-Mediterranean temperature. Journal of Geophysical Research: Atmospheres 128, e2023JD038712.
Monerie, P.-A., Oudar, T., Sanchez-Gomez, E., 2019. Respective impacts of Arctic sea ice decline and increasing greenhouse gases concentration on Sahel precipitation. Climate Dynamics 52, 5947-5964.
Monerie, P.-A., Sanchez-Gomez, E., Boé, J., 2017. On the range of future Sahel precipitation projections and the selection of a sub-sample of CMIP5 models for impact studies. Climate Dynamics 48, 2751-2770.
Moore, C.M., Mills, M.M., Arrigo, K.R., Berman-Frank, I., Bopp, L., Boyd, P.W., Galbraith, E.D., Geider, R.J., Guieu, C., Jaccard, S.L., Jickells, T.D., La Roche, J., Lenton, T.M., Mahowald, N.M., Marañón, E., Marinov, I., Moore, J.K., Nakatsuka, T., Oschlies, A., Saito, M.A., Thingstad, T.F., Tsuda, A., Ulloa, O., 2013. Processes and patterns of oceanic nutrient limitation. Nature Geoscience 6, 701-710.
Mulitza, S., Boltovskoy, D., Donner, B., Meggers, H., Paul, A., Wefer, G., 2003. Temperature:δ18O relationships of planktonic foraminifera collected from surface waters. Palaeogeography, Palaeoclimatology, Palaeoecology 202, 143-152.
Mulitza, S., Heslop, D., Pittauerova, D., Fischer, H.W., Meyer, I., Stuut, J.-B., Zabel, M., Mollenhauer, G., Collins, J.A., Kuhnert, H., Schulz, M., 2010. Increase in African dust flux at the onset of commercial agriculture in the Sahel region. Nature 466, 226-228.
Mulitza, S., Prange, M., Stuut, J.-B., Zabel, M., von Dobeneck, T., Itambi, A.C., Nizou, J., Schulz, M., Wefer, G., 2008. Sahel megadroughts triggered by glacial slowdowns of Atlantic meridional overturning. Paleoceanography 23, PA4206.
Müller, P.J., Fischer, G., 2001. A 4-year sediment trap record of alkenones from the filamentous upwelling region off Cape Blanc, NW Africa and a comparison with distributions in underlying sediments. Deep Sea Research Part I: Oceanographic Research Papers 48, 1877-1903.
Müller, P.J., Kirst, G., Ruhland, G., von Storch, I., Rosell-Melé, A., 1998. Calibration of the alkenone paleotemperature index U37K′ based on core-tops from the eastern South Atlantic and the global ocean (60°N-60°S). Geochimica et Cosmochimica Acta 62, 1757-1772.
Murakami, H., 2020. ATBD of GCOM-C chlorophyll-a concentration algorithm (version 2).
Naafs, B.D.A., Hefter, J., Acton, G., Haug, G.H., Martínez-Garcia, A., Pancost, R., Stein, R., 2012. Strengthening of North American dust sources during the late Pliocene (2.7 Ma). Earth and Planetary Science Letters 317–318, 8-19.
Naafs, B.D.A., Stein, R., Hefter, J., Khélifi, N., De Schepper, S., Haug, G.H., 2010. Late Pliocene changes in the North Atlantic Current. Earth and Planetary Science Letters 298, 434-442.
Nicholson, S.E., 2009. A revised picture of the structure of the ‘‘monsoon’’ and land ITCZ over West Africa. Climate Dynamics 32, 1155-1171.
O'Mara, N.A., Skonieczny, C., McGee, D., Winckler, G., Bory, A.J.-M., Bradtmiller, L.I., Malaizé, B., Polissar, P.J., 2024. Constraining Plio-Pleistocene Shifts in Northwest African Hydroclimate, Ecosystem Distributions, and Marine Productivity: New Paleo-Records Across the Mid-Pleistocene Transition. Paleoceanography and Paleoclimatology 39, e2023PA004777.

O'Mara, N.A., Skonieczny, C., McGee, D., Winckler, G., Bory, A.J.M., Bradtmiller, L.I., Malaizé, B., Polissar, P.J., 2022. Pleistocene drivers of Northwest African hydroclimate and vegetation. Nature Communications 13, 3552.
Ogg, J.G., 2012. Chapter 5 - Geomagnetic Polarity Time Scale, in: Gradstein, F.M., Ogg, J.G., Schmitz, M.D., Ogg, G.M. (Eds.), The Geologic Time Scale. Elsevier, Boston, pp. 85-113.
Park, J.-y., Bader, J., Matei, D., 2016. Anthropogenic Mediterranean warming essential driver for present and future Sahel rainfall. Nature Clim. Change 6, 941-945.
Peeters, F.J.C., Brummer, G.-J.A., Ganssen, G., 2002. The effect of upwelling on the distribution and stable isotope composition of Globigerina bulloides and Globigerinoides ruber (planktic foraminifera) in modern surface waters of the NW Arabian Sea. Global and Planetary Change 34, 269-291.
Peña-Izquierdo, J., Pelegrí, J.L., Pastor, M.V., Castellanos, P., Emelianov, M., Gasser, M., Salvador, J., Vázquez-Domínguez, E., 2012. The continental slope current system between Cape Verde and the Canary Islands. Sci. Mar 76, 65-78.
Price, N.B., Calvert, S.E., 1977. The contrasting geochemical behaviours of iodine and bromine in recent sediments from the Namibian shelf. Geochimica et Cosmochimica Acta 41, 1769-1775.
QGIS.org, 2024. QGIS Geographic Information System. QGIS Association.
Raffi, I., Backman, J., Fornaciari, E., Pälike, H., Rio, D., Lourens, L., Hilgen, F., 2006. A review of calcareous nannofossil astrobiochronology encompassing the past 25 million years. Quaternary Science Reviews 25, 3113-3137.
Raymo, M.E., Kozdon, R., Evans, D., Lisiecki, L., Ford, H.L., 2018. The accuracy of mid-Pliocene δ18O-based ice volume and sea level reconstructions. Earth-Science Reviews 177, 291-302.
Richardson, P.L., Walsh, D., 1986. Mapping climatological seasonal variations of surface currents in the tropical Atlantic using ship drifts. Journal of Geophysical Research: Oceans 91, 10537-10550.
Rohling, E.J., Foster, G.L., Gernon, T.M., Grant, K.M., Heslop, D., Hibbert, F.D., Roberts, A.P., Yu, J., 2022. Comparison and synthesis of sea-level and deep-sea temperature variations over the past 40 million years. Reviews of Geophysics 60, e2022RG000775.
Romero, O.E., Kim, J.-H., Donner, B., 2008. Submillennial-to-millennial variability of diatom production off Mauritania, NW Africa, during the last glacial cycle. Paleoceanography 23, PA3218.
Rosell-Melé, A., Prahl, F.G., 2013. Seasonality of UK′37 temperature estimates as inferred from sediment trap data. Quaternary Science Reviews 72, 128-136.
Rossignol-Strick, M., 1985. Mediterranean Quaternary sapropels, an immediate response of the African monsoon to variation of insolation. Palaeogeography, Palaeoclimatology, Palaeoecology 49, 237-263.
Ruddiman, W., Janecek, T., 1989. Pliocene-Pleistocene biogenic and terrigenous fluxes at equatorial Atlantic Sites 662, 663, and 664, Proc. Ocean Drill. Program Sci. Results, pp. 1-240.
Ruddiman, W.F., Sarnthein, M., Baldauf, J.G., et al., 1989. Proc. ODP, Init. Repts., 108. College Station, TX (Ocean Drilling Program).
Ruggieri, E., 2013. A Bayesian approach to detecting change points in climatic records. International Journal of Climatology 33, 520-528.
Sarnthein, M., Thiede, J., Pflaumann, U., Erlenkeuser, H., Fütterer, D., Koopmann, B., Lange, H., Seibold, E., 1982. Atmospheric and Oceanic Circulation Patterns off Northwest Africa During the Past 25 Million Years, in: von Rad, U., Hinz, K., Sarnthein, M., Seibold, E. (Eds.), Geology of the Northwest African Continental Margin. Springer Berlin Heidelberg, Berlin, Heidelberg, pp. 545-604.
Scheff, J., Frierson, D., 2012. Twenty-First-Century Multimodel Subtropical Precipitation Declines Are Mostly Midlatitude Shifts. Journal of Climate 25, 4330-4347.
Schlosser, C., Klar, J.K., Wake, B.D., Snow, J.T., Honey, D.J., Woodward, E.M.S., Lohan, M.C., Achterberg, E.P., Moore, C.M., 2014. Seasonal ITCZ migration dynamically controls the location of the (sub)tropical Atlantic biogeochemical divide. Proceedings of the National Academy of Sciences 111, 1438-1442.
Sigman, D.M., Jaccard, S.L., Haug, G.H., 2004. Polar ocean stratification in a cold climate. Nature 428, 59-63.
Sikes, E., Farrington, J.t., Keigwin, L., 1991. Use of the alkenone unsaturation ratio U37K to determine past sea surface temperatures: core-top SST calibrations and methodology considerations. Earth and Planetary Science Letters 104, 36-47.
Skonieczny, C., Bory, A., Bout-Roumazeilles, V., Abouchami, W., Galer, S.J.G., Crosta, X., Diallo, A., Ndiaye, T., 2013. A three-year time series of mineral dust deposits on the West African margin: Sedimentological and geochemical signatures and implications for interpretation of marine paleo-dust records. Earth and Planetary Science Letters 364, 145-156.

Skonieczny, C., McGee, D., Winckler, G., Bory, A., Bradtmiller, L.I., Kinsley, C.W., Polissar, P.J., De Pol-Holz, R., Rossignol, L., Malaizé, B., 2019. Monsoon-driven Saharan dust variability over the past 240,000 years. Science Advances 5, eaav1887.
Steph, S., Regenberg, M., Tiedemann, R., Mulitza, S., Nürnberg, D., 2009. Stable isotopes of planktonic foraminifera from tropical Atlantic/Caribbean core-tops: Implications for reconstructing upper ocean stratification. Marine Micropaleontology 71, 1-19.
Stramma, L., England, M., 1999. On the water masses and mean circulation of the South Atlantic Ocean. Journal of Geophysical Research: Oceans 104, 20863-20883.
Stuut, J.-B., Zabel, M., Ratmeyer, V., Helmke, P., Schefuß, E., Lavik, G., Schneider, R., 2005. Provenance of present-day eolian dust collected off NW Africa. Journal of Geophysical Research: Atmospheres 110, D04202.
Thomas, N., Nigam, S., 2018. Twentieth-Century Climate Change over Africa: Seasonal Hydroclimate Trends and Sahara Desert Expansion. Journal of Climate 31, 3349-3370.
Tiedemann, R., Sarnthein, M., Shackleton, N.J., 1994. Astronomic timescale for the Pliocene Atlantic δ18O and dust flux records of Ocean Drilling Program Site 659. Paleoceanography 9, 619-638.
Tierney, J.E., Tingley, M.P., 2018. BAYSPLINE: A New Calibration for the Alkenone Paleothermometer. Paleoceanography and Paleoclimatology 33, 281-301.
Tjallingii, R., Claussen, M., Stuut, J.-B.W., Fohlmeister, J., Jahn, A., Bickert, T., Lamy, F., Rohl, U., 2008. Coherent high- and low-latitude control of the northwest African hydrological balance. Nature Geosci 1, 670-675.
Tolderlund, D.S., Bé, A.W.H., 1971. Seasonal Distribution of Planktonic Foraminifera in the Western North Atlantic. Micropaleontology 17, 297-329.
Trauth, M.H., Larrasoaña, J.C., Mudelsee, M., 2009. Trends, rhythms and events in Plio-Pleistocene African climate. Quaternary Science Reviews 28, 399-411.
Trenberth, K.E., 1998. Atmospheric Moisture Residence Times and Cycling: Implications for Rainfall Rates and Climate Change. Climatic Change 39, 667-694.
Tuenter, E., Weber, S.L., Hilgen, F.J., Lourens, L.J., 2003. The response of the African summer monsoon to remote and local forcing due to precession and obliquity. Global and Planetary Change 36, 219-235.
Vallé, F., Dupont, L.M., Leroy, S.A.G., Schefuß, E., Wefer, G., 2014. Pliocene environmental change in West Africa and the onset of strong NE trade winds (ODP Sites 659 and 658). Palaeogeography, Palaeoclimatology, Palaeoecology 414, 403-414.
van der Does, M., Brummer, G.-J.A., Korte, L.F., Stuut, J.-B.W., 2021. Seasonality in Saharan Dust Across the Atlantic Ocean: From Atmospheric Transport to Seafloor Deposition. Journal of Geophysical Research: Atmospheres 126, e2021JD034614.
van der Weijst, C.M.H., Winkelhorst, J., de Nooijer, W., von der Heydt, A., Reichart, G.J., Sangiorgi, F., Sluijs, A., 2022. Pliocene evolution of the tropical Atlantic thermocline depth. Clim. Past 18, 961-973.
Vellinga, M., Wu, P., 2004. Low-Latitude Freshwater Influence on Centennial Variability of the Atlantic Thermohaline Circulation. Journal of Climate 17, 4498-4511.
Voelker, A.H.L., Colman, A., Olack, G., Waniek, J.J., Hodell, D., 2015. Oxygen and hydrogen isotope signatures of Northeast Atlantic water masses. Deep Sea Research Part II: Topical Studies in Oceanography 116, 89-106.
Volkman, J.K., 2000. Ecological and environmental factors affecting alkenone distributions in seawater and sediments. Geochemistry, Geophysics, Geosystems 1.
Wade, B.S., Pearson, P.N., Berggren, W.A., Pälike, H., 2011. Review and revision of Cenozoic tropical planktonic foraminiferal biostratigraphy and calibration to the geomagnetic polarity and astronomical time scale. Earth-Science Reviews 104, 111-142.
Wang, L., Sarnthein, M., Duplessy, J.-C., Erlenkeuser, H., Jung, S., Pflaumann, U., 1995. Paleo sea surface salinities in the low-latitude Atlantic: The δ18O record of Globigerinoides ruber (white). Paleoceanography 10, 749-761.
Wang, L.-C., Jin, F.-F., Wu, C.-R., Hsu, H.-H., 2017. Dynamics of upwelling annual cycle in the equatorial Atlantic Ocean. Geophysical Research Letters 44, 3737-3743.
Weltje, G.J., Bloemsma, M., Tjallingii, R., Heslop, D., Röhl, U., Croudace, I.W., 2015. Prediction of geochemical composition from XRF core scanner data: a new multivariate approach including automatic selection of calibration samples and quantification of uncertainties, in: Croudace;, I.W., Rothwell, R.G. (Eds.), Micro-XRF Studies of Sediment Cores. Springer, pp. 507-534.
Westerhold, T., Marwan, N., Drury, A.J., Liebrand, D., Agnini, C., Anagnostou, E., Barnet, J.S.K., Bohaty, S.M., De Vleeschouwer, D., Florindo, F., Frederichs, T., Hodell, D.A., Holbourn, A.E., Kroon, D., Lauretano, V., Littler, K., Lourens, L.J., Lyle, M., Pälike, H., Röhl, U., Tian, J., Wilkens, R.H., Wilson, P.A., Zachos, J.C., 2020. An astronomically dated record of Earth's climate and its predictability over the last 66 million years. Science 369, 1383-1387.

Wilkens, R.H., Westerhold, T., Drury, A.J., Lyle, M., Gorgas, T., Tian, J., 2017. Revisiting the Ceara Rise, equatorial Atlantic Ocean: isotope stratigraphy of ODP Leg 154 from 0 to 5 Ma. Clim. Past 13, 779-793.
Wit, J.C., Reichart, G.-J., A Jung, S.J., Kroon, D., 2010. Approaches to unravel seasonality in sea surface temperatures using paired single-specimen foraminiferal δ18O and Mg/Ca analyses. Paleoceanography 25.
Wycech, J.B., Rajagopalan, B., Molnar, P.H., Gill, E., Marchitto, T.M., 2022. Multiproxy Reconstruction of Pliocene North Atlantic Sea Surface Temperatures and Implications for Rainfall in North Africa. Paleoceanography and Paleoclimatology 37, e2022PA004424.
Yost, C.L., Ivory, S.J., Deino, A.L., Rabideaux, N.M., Kingston, J.D., Cohen, A.S., 2020. Phytoliths, pollen, and microcharcoal from the Baringo Basin, Kenya reveal savanna dynamics during the Plio-Pleistocene transition. Palaeogeography, Palaeoclimatology, Palaeoecology, 109779.
Yu, H., Tan, Q., Chin, M., Remer, L.A., Kahn, R.A., Bian, H., Kim, D., Zhang, Z., Yuan, T., Omar, A.H., Winker, D.M., Levy, R.C., Kalashnikova, O., Crepeau, L., Capelle, V., Chédin, A., 2019. Estimates of African Dust Deposition Along the Trans-Atlantic Transit Using the Decadelong Record of Aerosol Measurements from CALIOP, MODIS, MISR, and IASI. Journal of Geophysical Research: Atmospheres 124, 7975-7996.
Zhang, S., Stier, P., Dagan, G., Zhou, C., Wang, M., 2023. Sea surface warming patterns drive hydrological sensitivity uncertainties. Nature Climate Change 13, 545-553.
Zhang, X., Zwiers, F.W., Hegerl, G.C., Lambert, F.H., Gillett, N.P., Solomon, S., Stott, P.A., Nozawa, T., 2007. Detection of human influence on twentieth-century precipitation trends. Nature 448, 461-465.
Zhang, Z., Li, G., 2022. Uncertainty in the projected changes of Sahel summer rainfall under global warming in CMIP5 and CMIP6 multi-model ensembles. Climate Dynamics 59, 3579-3597.
Zhao, M., Beveridge, N.A.S., Shackleton, N.J., Sarnthein, M., Eglinton, G., 1995. Molecular stratigraphy of cores off northwest Africa: Sea surface temperature history over the last 80 Ka. Paleoceanography 10, 661-675.
Ziegler, M., Jilbert, T., de Lange, G.J., Lourens, L.J., Reichart, G.-J., 2008. Bromine counts from XRF scanning as an estimate of the marine organic carbon content of sediment cores. Geochemistry, Geophysics, Geosystems 9, Q05009.